LETTER

Quantitative phosphoproteomic analysis of the molecular substrates of sleep need

Zhiqiang Wang[1], Jing Ma[1], Chika Miyoshi[1], Yuxin Li[2], Makito Sato[1], Yukino Ogawa[1], Tingting Lou[1], Chengyuan Ma[3], Xue Gao[3], Chiyu Lee[1], Tomoyuki Fujiyama[1], Xiaojie Yang[1], Shuang Zhou[3], Noriko Hotta-Hirashima[1], Daniela Klewe-Nebenius[1], Aya Ikkyu[1], Miyo Kakizaki[1], Satomi Kanno[1], Liqin Cao[1], Satoru Takahashi[4], Junmin Peng[2], Yonghao Yu[5], Hiromasa Funato[1,6]*, Masashi Yanagisawa[1,7,8]* & Qinghua Liu[1,3,9,10]*

Sleep and wake have global effects on brain physiology, from molecular changes[1–4] and neuronal activities to synaptic plasticity[3–7]. Sleep–wake homeostasis is maintained by the generation of a sleep need that accumulates during waking and dissipates during sleep[8–11]. Here we investigate the molecular basis of sleep need using quantitative phosphoproteomic analysis of the sleep-deprived and *Sleepy* mouse models of increased sleep need. Sleep deprivation induces cumulative phosphorylation of the brain proteome, which dissipates during sleep. *Sleepy* mice, owing to a gain-of-function mutation in the *Sik3* gene[12], have a constitutively high sleep need despite increased sleep amount. The brain proteome of these mice exhibits hyperphosphorylation, similar to that seen in the brain of sleep-deprived mice. Comparison of the two models identifies 80 mostly synaptic sleep-need-index phosphoproteins (SNIPPs), in which phosphorylation states closely parallel changes of sleep need. SLEEPY, the mutant SIK3 protein, preferentially associates with and phosphorylates SNIPPs. Inhibition of SIK3 activity reduces phosphorylation of SNIPPs and slow wave activity during non-rapid-eye-movement sleep, the best known measurable index of sleep need, in both *Sleepy* mice and sleep-deprived wild-type mice. Our results suggest that phosphorylation of SNIPPs accumulates and dissipates in relation to sleep need, and therefore SNIPP phosphorylation is a molecular signature of sleep need. Whereas waking encodes memories by potentiating synapses, sleep consolidates memories and restores synaptic homeostasis by globally downscaling excitatory synapses[4–6]. Thus, the phosphorylation–dephosphorylation cycle of SNIPPs may represent a major regulatory mechanism that underlies both synaptic homeostasis and sleep–wake homeostasis.

Homeostatic sleep regulation is a global, intrinsic and cumulative process that ultimately involves most brain cells and regions[3,5,7]; this is distinct from executive switching between sleep and wake states, which is controlled by specific neural circuits[13,14]. We hypothesize that the molecular substrates of sleep need satisfy four criteria: 1) they should be globally and similarly regulated in most brain cells or regions; 2) they should accumulate gradually during waking and dissipate through sleep; 3) they should change in parallel with sleep need in different contexts; and 4) gain or loss of these functions should cause bidirectional changes of sleep need.

Sleep deprivation increases sleep need in mice, as shown by enhanced slow wave activity (SWA) or delta power (1–4 Hz) of electroencephalography (EEG) during non-rapid-eye-movement sleep (NREMS), which declines rapidly to the baseline followed by rebound sleep in early dark phase[8,10,12] (Fig. 1a, Extended Data Fig. 1a–e). We recently identified a dominant mutation in *Sleepy* mice[12], *Sik3*[Slp/+], in which a single nucleotide substitution in the gene for salt-inducible kinase 3 (SIK3), a member of the AMP-activated protein kinase (AMPK) family[15], causes constitutively high sleep need, manifested by elevated SWA and duration of NREMS (Extended Data Fig. 1f–i). Sleep deprivation increases wake time, whereas the *Sleepy* mutation decreases wake time; yet both cause elevated sleep need. We hypothesized that cross-comparison of these contrasting models of increased sleep need would reveal specific molecular changes associated with sleep need by filtering out non-specific effects of prolonged sleep, wake and stress.

We subjected three groups of wild-type C57BL/6N mice, at Zeitgeber time (ZT) zero, to 6 h of ad libitum sleep (S6) or sleep deprivation (SD6), or 6 h of sleep deprivation followed by a 3-h recovery sleep (RS3), respectively (Fig. 1a). We collected brains from wild-type (*Sik3*^{+/+}) and *Sleepy* (*Sik3*[Slp/+]) mice at ZT12.5, the lowest point of SWA in wild-type mice (Fig. 1a). As shown by immunoblotting with antibodies against 14 phosphorylated substrate motifs, global phosphorylation of substrates of AMPK, protein kinase C (PKC), protein kinase A (PKA) and 'ataxia telangiectasia mutated' (ATM) and 'ATM and RAD3-related' (ATR) kinases was specifically increased in brains of both *Sleepy* mice and wild-type SD6 mice, but was not affected by fasting (Fig. 1b, c and Extended Data Figs. 2, 3). By contrast, other signalling pathways, such as casein kinase II (CK2) or tyrosine kinases, were not significantly affected (Fig. 1c and Extended Data Fig. 2). These observations indicate that similar kinase pathways are globally activated in *Sleepy* and sleep-deprived brains.

Next, we performed quantitative proteomic and phosphoproteomic studies of whole brain lysates using multiplex tandem mass tag (TMT) labelling coupled with liquid chromatography–mass spectrometry (LC–MS)[16–19] (Fig. 1a). A total of 4 proteomic and 13 phosphoproteomic experiments was performed (Supplementary Tables 1, 2). The amount of peptides or phosphopeptides corresponding to exon 13, which is not translated in the *Sik3*[Slp] mutant allele, was specifically reduced by 40% in *Sik3*[Slp/+] relative to *Sik3*^{+/+} samples (Fig. 1d, g and Extended Data Fig. 4a); this acted as a stringent internal control. In summary, brain proteomic analysis quantified 7,963 proteins, of which 5,280 were present in all conditions in the pairwise comparisons of SD6 and RS3 (5,769 proteins), SD6 and S6 (6,067 proteins), and *Sleepy* and wild-type (7,650 proteins) groups (Extended Data Fig. 4b–h, Supplementary Table 1). Phosphoproteomic analysis quantified a total of 62,384 unique phosphopeptides from 7,104 phosphoproteins and identified 51,821 phosphorylation sites (Supplementary Table 2a).

Few quantified peptides or proteins showed significant changes in abundance ($Q < 0.2$) in the comparisons of brain proteomes between *Sleepy* and wild-type (0.09%; 3.5%), SD6 and RS3 (0.01%; 0%), or SD6 and S6 (0%; 0.01%) samples (Fig. 1d–f and Extended Data

Fig. 1 | Brains of *Sleepy* mutant mice exhibit hyperphosphorylation that mimics that in sleep-deprived brains. a, Experimental design for proteomic and phosphoproteomic analysis of two models. **b**, Representative immunoblots of brain lysates with antibody specific for AMPK target phosphorylation motifs. Blots represent three (sleep-deprived) or two (*Sleepy*) independent experiments. **c**, Quantitative analysis of immunoblots using specific antibodies for different phosphorylated protein motifs. $n = 12$ (S6), 9 (SD6, RS3), 6 (wild-type (WT), *Sleepy* (Slp)). Mean ± s.d., two-way ANOVA, Fisher's least significant difference (LSD). **d–i**, Volcano plots showing changes in peptides (**d–f**) and phosphopeptides (**g–i**) in *Sleepy*/wild-type, SD6/RS3 and SD6/S6 comparisons. Multiple unpaired *t*-test (*P* value) followed by false discovery rate (FDR) (*Q* value) analysis. In, increase; De, decrease. **j**, Venn diagram of significantly changed phosphopeptides among three groups, with the number of significantly changed phosphopeptides in each experiment shown in parentheses. **k**, Analysis of mean abundance of 918 phosphopeptides that are changed in both SD6/RS3 and SD6/S6 comparisons. Mean, one-way ANOVA, Dunnett's test. **l**, Hierarchical cluster analysis of 329 phosphopeptides that are changed in all three groups. *$P < 0.05$; ‡$P < 0.001$; NS, not significant ($P > 0.05$).

Fig. 4g), suggesting that the whole brain proteome was globally stable (Supplementary Discussion 1). By contrast, comparison of the brain phosphoproteomes showed that a sizable portion of phosphopeptides exhibited significant changes ($Q < 0.2$) between the SD6 and RS3 (12.4%), SD6 and S6 (4%), and *Sleepy* and wild-type (18.3%) conditions (Fig. 1g–j). In sleep-deprived brains, the majority of changes in phosphorylation are increases: SD6/RS3 (3,551/4,293, 82.7%) or SD6/S6 (1,198/1,381, 86.7%) (Fig. 1h, i). The mean abundance of 918 phosphopeptides that were changed in both SD6/RS3 and SD6/S6 groups was around 32% or around 25% lower in S6 or RS3 brains, respectively, than in SD6 brains (Fig. 1j, k). This asymmetric increase in phosphorylation was not observed in the liver phosphoproteome after sleep deprivation (Extended Data Fig. 5). Instead, the liver phosphoproteome showed decreases in global phosphorylation in these comparisons: SD6/S6 (1,275/2,186, 58.3%) and SD6/RS3 (286/433, 66.1%) (Extended Data Fig. 5b, c). These studies suggest that sleep and wake have opposing effects on the brain phosphoproteome: prolonged wakefulness causes hyperphosphorylation, whereas sleep promotes global dephosphorylation of the brain proteome.

Comparison of *Sleepy* and sleep-deprived models reveals 329 phosphopeptides that are significantly ($Q < 0.2$) altered in all three (*Sleepy*/

wild-type, SD6/S6 and SD6/RS3) comparisons (Fig. 1j). On the basis of the mean abundance of each of these 329 phosphopeptides, unsupervised cluster analysis groups *Sleepy* samples with SD6 samples, whereas wild-type samples cluster with S6 and RS3 samples (Fig. 1l). We used antibodies against specific phosphorylation sites to confirm hyperphosphorylation of multiple proteins in both *Sleepy* and SD6 samples (Extended Data Fig. 4i, j). These results suggest that *Sleepy* mutant brains exhibit a global hyperphosphorylation of proteins, mimicking that seen in sleep-deprived brains.

Protein functions can be switched on or off by site-specific phosphorylation, or modulated by cumulative phosphorylation of multiple sites[20–23]. We noted a group of proteins containing multiple phosphorylation sites that appear to be co-ordinately regulated in both *Sleepy* and SD6 models (Extended Data Fig. 6a, b). For example, the synaptic vesicle protein synapsin-1 contains multiple functionally important phosphorylation sites[21,22], almost all of which are hyperphosphorylated in brains of sleep-deprived or *Sleepy* mice (Fig. 2a and Extended Data Fig. 6a). We measured overall phosphorylation state change (ΔPs) of synapsin-1 by calculating the sum of $\log_2$(fold change) values of all significantly ($Q < 0.2$) changed synapsin-1 phosphopeptides. Synapsin-1 has ΔPs values of 7.5, 5.5 and 13.7 in the SD6/RS3,

Fig. 2 | Changes in phosphorylation state of SNIPPs parallel changes in sleep need.
a, Volcano plots of quantified phosphopeptides of synapsin-1 in SD6/RS3 (violet), SD6/S6 (blue) and *Sleepy*/wild-type (orange) comparisons. Multiple unpaired *t*-test (*P* value) followed by FDR (*Q* value) analysis. **b**, Phosphorylation of synapsin-1 was assessed by regular or phospho-tag SDS–PAGE followed by immunoblotting (two independent experiments). **c–e**, Global ΔPs analysis of phosphoproteins in three comparisons. Numbers of hyperphosphorylated (Hyper) and hypophosphorylated (Hypo) peptides in each comparison are shown. Labels show genes encoding the proteins. Dotted lines, ΔPs $= \pm 2.4$. **f**, Percentage of synaptic proteins in total, hypophosphorylated and hyperphosphorylated proteins, and among 80 SNIPPs. χ^2 test, two-sided. **g**, Mutations in 12 SNIPP genes cause sleep phenotypes. Genes for synaptic proteins are shown in bold. **h**, A schematic of the normal sleep–wake model[4]. **i**, Quantitative ΔPs analysis of SNIPPs in the W4/S4 model. $n = 966$ (total), 62 (SNIPPs). Mean; unpaired *t*-test, two-tailed. ‡$P < 0.001$.
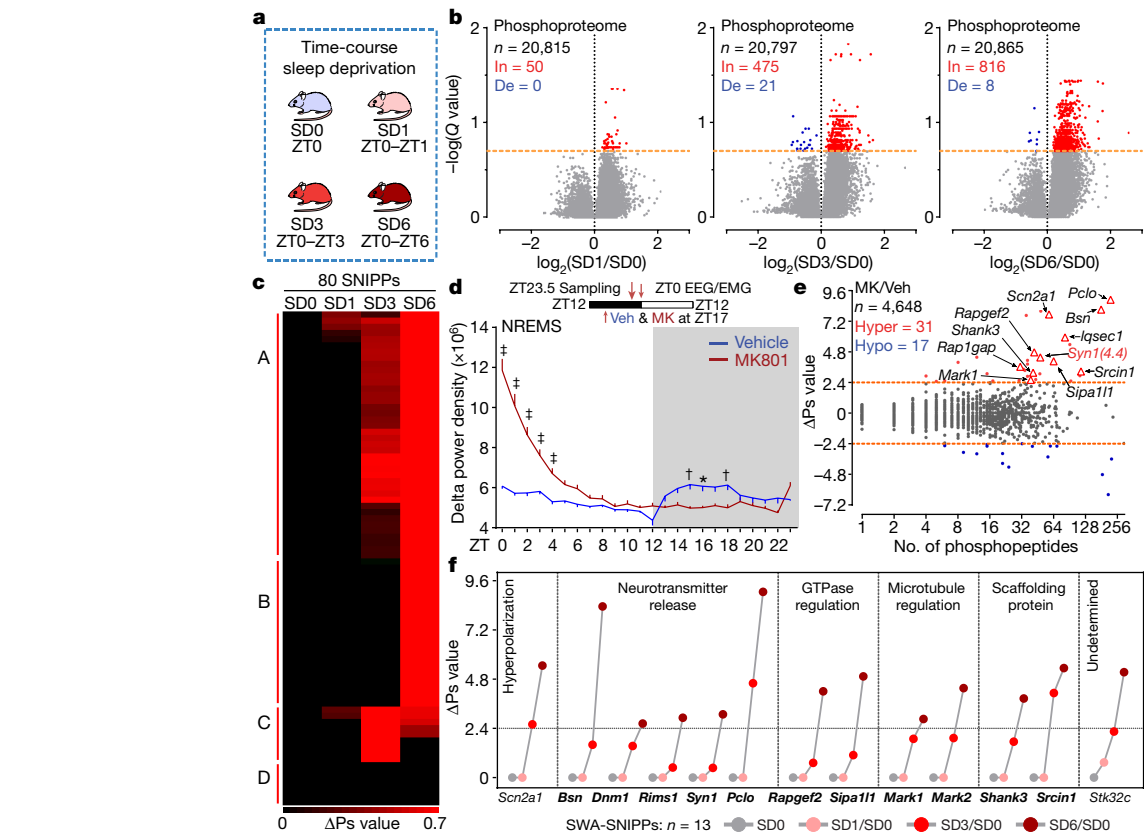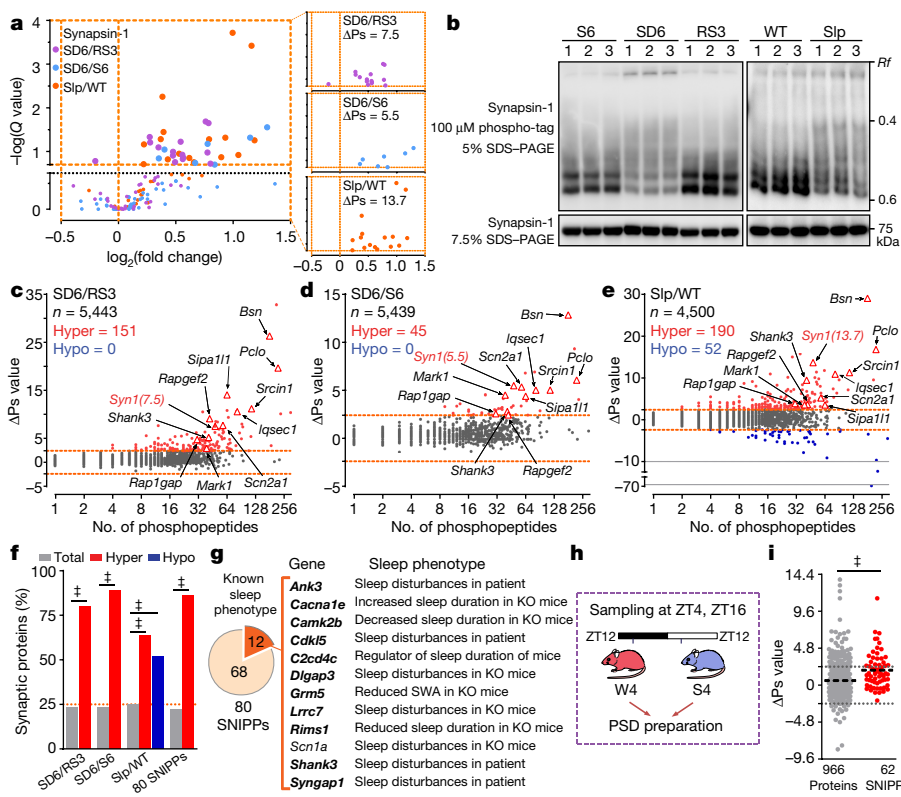
Fig. 3 | SNIPPs exhibit time-dependent cumulative phosphorylation.
a, A schematic of time-course sleep deprivation. **b**, Volcano plots comparing phosphoproteomes of SD1/SD0, SD3/SD0 and SD6/SD0. Multiple unpaired *t*-test (*P* value) followed by FDR (*Q* value) analysis. **c**, Temporal profile and classification of phosphorylation-state changes of SNIPPs. **d**, Circadian analysis of absolute NREMS delta power of vehicle (Veh) or MK801 (MK)-injected mice ($n = 14$). Mean $\pm$ s.e.m., two-way ANOVA, Sidak's test *$P < 0.05$; †$P < 0.01$; ‡$P < 0.001$. **e**, Global ΔPs analysis of MK801/vehicle group. **f**, Time-dependent cumulative phosphorylation of 13 SWA-SNIPPs that occur in *Sleepy*, SD and MK801 models. Genes encoding synaptic proteins are shown in bold.
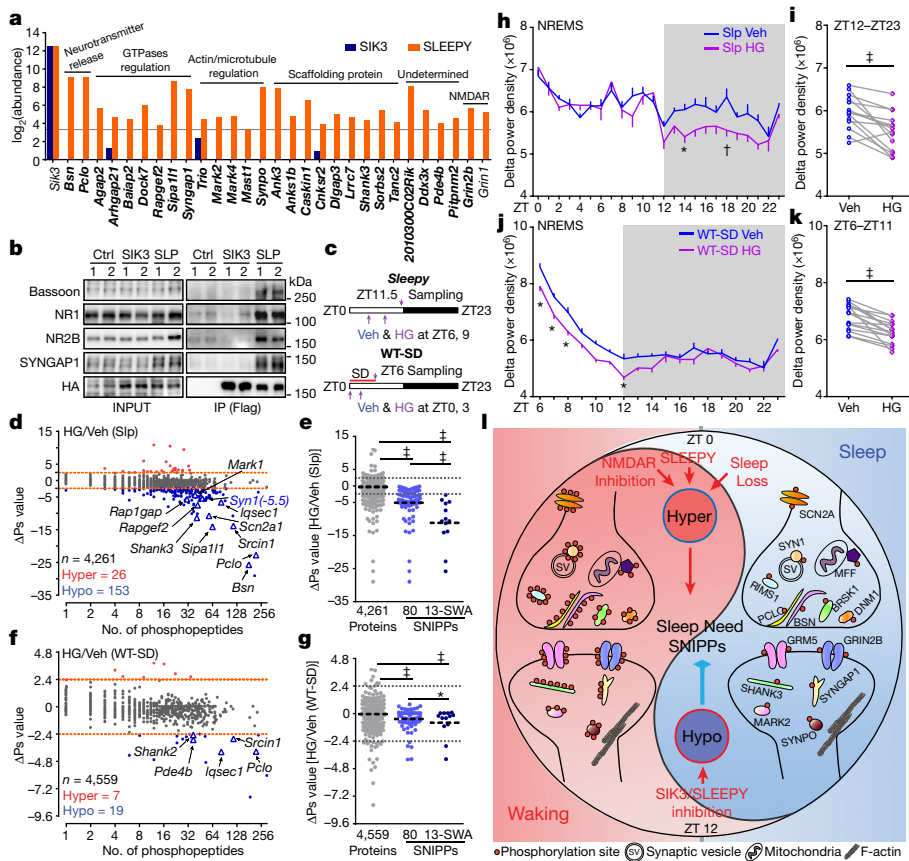
Fig. 4 | SLEEPY preferentially interacts with SNIPPs and alters sleep–wake homeostasis. a, Comparison of mass-spectrometry signals of SNIPPs in immunoprecipitates of SLEEPY and SIK3. **b,** Immunoprecipitation confirms interactions between SLEEPY and SNIPPs (two independent experiments). **c,** A schematic of SIK3 inhibition in *Sleepy* and sleep-deprived wild-type (WT-SD) mice. Veh, vehicle; HG, HG-9-91-01. **d–g,** Global (**d, f**) and quantitative (**e, g**) ΔPs analysis of HG/vehicle (Slp) and HG/vehicle (WT-SD) groups. **h–k,** Circadian (**h, j**) and mean (**i, k**) absolute NREMS delta power analysis of HG/vehicle *Sleepy* ($n = 14$) and HG/vehicle WT-SD ($n = 16$) groups. **l,** Molecular model of synaptic homeostasis and sleep–wake homeostasis. Mean, one-way ANOVA, Tukey's test (**e, g**); Mean ± s.e.m., two-way ANOVA, Sidak's test (**h, j**); Paired *t*-test, two-tailed (**i, k**). *$P < 0.05$; †$P < 0.01$; ‡$P < 0.001$.

SD6/S6 and *Sleepy*/wild-type comparisons, respectively (Fig. 2a). Hyperphosphorylation of synapsin-1 in *Sleepy* and SD6 brain lysates was confirmed by phospho-tag gel electrophoresis (Fig. 2b).

Next, we performed global phosphorylation state change analysis for all quantified phosphoproteins in our datasets (Fig. 2c–e and Supplementary Table 3). In the sleep-deprived model, the phosphorylation state of 151 and 45 proteins is significantly upregulated (hyperphosphorylated, ΔPs > 2.4) in SD6 brains relative to RS3 or S6 brains, respectively (Fig. 2c, d). The phosphorylation state of 190 proteins is significantly upregulated, whereas the phosphorylation state of 52 proteins is downregulated (hypophosphorylation, ΔPs < −2.4) in the brains of *Sleepy* mice in comparison to those of wild-type mice (Fig. 2e). Cross-comparison of sleep-deprived and *Sleepy* models identified 80 hyperphosphorylated proteins, which we termed the sleep-need-index-phosphoproteins (SNIPPs), whose cumulative changes in phosphorylation state parallel those of sleep need in both models (Extended Data Fig. 7a).

Notably, 69 (>86%) of the 80 SNIPPs are annotated as synaptic proteins (Fig. 2f, Extended Data Fig. 7b and Supplementary Table 4a, b), whereas only 20% of the total phosphoproteins are annotated as synaptic proteins. A literature search reveals that mutations of 12 (15%) of the 80 SNIPPs cause sleep phenotypes in mice or humans (Fig. 2g and Supplementary Table 4a). Furthermore, we analysed published phosphoproteomic data of post-synaptic density (PSD) fractions from mouse forebrains collected in normal sleep (S4) and wake (W4) states[4] (Fig. 2h and Supplementary Table 5). Approximately 70% of phosphorylation changes observed in PSD fractions are increases, and the mean ΔPs value of the 80 SNIPPs is significantly increased in accordance with higher sleep need in wake brains relative to sleep brains (Fig. 2i and Extended Data Fig. 6c, d). These observations suggest a potential mechanistic link between the synaptic phosphoproteome and homeostatic sleep regulation (Supplementary Discussion 2).

Because synaptic activities underlie waking experience, we hypothesize that SNIPPs track waking experience through cumulative phosphorylation. To test this hypothesis, we conducted a time-course

sleep deprivation followed by quantitative phosphoproteomic analysis (Fig. 3a). Comparison of SD1, SD3 or SD6 and SD0 samples reveals a time-dependent increase in the number of phosphorylation events in whole-brain phosphoproteome (Fig. 3b). ΔPs analysis indicates that the mean phosphorylation states of 80 SNIPPs gradually rise with the duration of sleep deprivation (Extended Data Fig. 6e), with many SNIPPs showing time-dependent cumulative phosphorylation (Fig. 3c, class A–C).

MK801, a specific inhibitor of *N*-methyl-D-aspartate receptor (NMDAR), has previously been identified as a potent inducer of SWA in rodents[24–26]. Our quantitative phosphoproteomic analysis of this pharmacological model identified 31 hyperphosphorylated proteins (ΔPs > 2.4) in the MK801 model compared to vehicle-only control, of which 25 (80%) are annotated as synaptic proteins (Fig. 3d, e and Extended Data Fig. 8). The MK801, *Sleepy* and sleep-deprived models have 21 SNIPPs in common (Extended Data Fig. 8j), 13 of which accumulate phosphorylation in a time-dependent manner (Fig. 3f). These 13 SWA-SNIPPs not only serve as a reliable molecular indicator of SWA or sleep need in multiple models, but also may contribute critically to regulation of SWA, a macro-electrophysiological readout of synaptic functions[5,7] (Supplementary Discussion 3).

To examine whether SNIPPs are substrates of SLEEPY (the protein encoded by *Sik3^Slp*), we compared the interactomes of SLEEPY and wild-type SIK3 by immunoprecipitation and mass spectrometric analysis using whole-brain lysates from Flag-HA-*Sik3^Slp* and Flag-HA-*Sik3^+* knock-in mice[12] (Extended Data Fig. 9a and Supplementary Table 6). SLEEPY preferentially associated with synaptic proteins, including 28 of 80 SNIPPs (Fig. 4a and Extended Data Fig. 9b, c). Immunoprecipitation and western blotting confirmed enhanced associations between SLEEPY and SNIPPs such as the pre-synaptic active zone protein bassoon, synaptic RAS GTPase-activating protein 1 (SYNGAP1) and NMDAR subunits NR2B and NR1 (Fig. 4b).

We applied the AMPK Motif Analyzer to predict 2,943 phosphopeptides as potential AMPK substrates[27] in the *Sleepy*/wild-type phosphoproteome dataset (Extended Data Fig. 9d and Supplementary

Table 4c). Among these, 625 phosphopeptides were significantly changed ($Q < 0.2$) in *Sleepy* brains in comparison to wild-type brains, 462 of which were hyperphosphorylated in *Sleepy* brains (Extended Data Fig. 9d). The 28 SNIPPs that interact with SLEEPY contain 47 putative AMPK sites that are differently phosphorylated in *Sleepy* brains, of which 40 (85%) are hyperphosphorylated in *Sleepy* brains (Extended Data Fig. 9e). Recombinant SLEEPY and SIK3 exhibited similar in vitro kinase activities (Extended Data Fig. 9f), suggesting that SLEEPY itself does not have increased kinase activity. Taken together, these observations suggest that SLEEPY may increase phosphorylation of SNIPPs by enhancing kinase–substrate association.

Next, we attempted to rescue the phenotypes of *Sleepy* mice by intracerebroventricular injection of the pan-SIK inhibitor HG-9-91-01[28] (HG) to inhibit SLEEPY or SIK3 kinase activity (Fig. 4c). Administration of HG significantly reduced phosphorylation of AMPK substrates, particularly phosphorylation of the 28 SLEEPY-interacting SNIPPs (Extended data Fig. 9g–i). Consistent with this, HG treatment of *Sleepy* mice reduced phosphorylation of SNIPPs and SWA, but not duration, of NREMS (Fig. 4d, e, h, i and Extended Data Fig. 9j–m). Similarly, HG treatment of sleep-deprived wild-type mice reduced phosphorylation of AMPK substrates, phosphorylation of SNIPPs and SWA of NREMS (Fig. 4f, g, j, k and Extended Data Fig. 10), suggesting that SIK3 and SNIPPs have a critical role in normal homeostatic sleep regulation.

We hypothesize that a core set of SNIPPs monitor the duration and richness of prior waking through cumulative phosphorylation, which translates into a corresponding sleep need that determines the quality and duration of subsequent sleep[11] (Fig. 4l and Supplementary Discussion 4). Whereas prolonged wakefulness leads to cognitive impairment and sleepiness, sleep refreshes the brain through multiple restorative effects and optimizes cognitive functions for the next waking period[5,7,9,11]. Specifically, the synaptic homeostasis hypothesis posits that waking encodes memories by potentiating synapses, whereas sleep consolidates memories and restores synaptic homeostasis by global downscaling of synaptic strength[5]. We hypothesize that the phosphorylation–dephosphorylation cycle of SNIPPs represent a major regulatory mechanism that underlies both synaptic homeostasis and sleep–wake homeostasis to maximize cognitive functions of the brain.

Online content

Any Methods, including any statements of data availability and Nature Research reporting summaries, along with any additional references and Source Data files, are available in the online version of the paper at https://doi.org/10.1038/s41586-018-0218-8.

1. Cirelli, C. & Tononi, G. Changes in anti-phosphoserine and anti-phosphothreonine antibody binding during the sleep-waking cycle and after lesions of the locus coeruleus. *Sleep Res. Online* **1**, 11–18 (1998).
2. Elliott, A. S., Huber, J. D., O'Callaghan, J. P., Rosen, C. L. & Miller, D. B. A review of sleep deprivation studies evaluating the brain transcriptome. *Springerplus* **3**, 728 (2014).
3. Thompson, C. L. et al. Molecular and anatomical signatures of sleep deprivation in the mouse brain. *Front. Neurosci.* **4**, 165 (2010).
4. Diering, G. H. et al. Homer1a drives homeostatic scaling-down of excitatory synapses during sleep. *Science* **355**, 511–515 (2017).
5. Tononi, G. & Cirelli, C. Sleep and the price of plasticity: from synaptic and cellular homeostasis to memory consolidation and integration. *Neuron* **81**, 12–34 (2014).
6. de Vivo, L. et al. Ultrastructural evidence for synaptic scaling across the wake/sleep cycle. *Science* **355**, 507–510 (2017).
7. Vyazovskiy, V. V. & Harris, K. D. Sleep and the single neuron: the role of global slow oscillations in individual cell rest. *Nat. Rev. Neurosci.* **14**, 443–451 (2013).
8. Borbely, A. A. A two process model of sleep regulation. *Hum. Neurobiol.* **1**, 195–204 (1982).
9. Benington, J. H. Sleep homeostasis and the function of sleep. *Sleep* **23**, 959–966 (2000).
10. Franken, P., Chollet, D. & Tafti, M. The homeostatic regulation of sleep need is under genetic control. *J. Neurosci.* **21**, 2610–2621 (2001).
11. Vassalli, A. & Dijk, D. J. Sleep function: current questions and new approaches. *Eur. J. Neurosci.* **29**, 1830–1841 (2009).
12. Funato, H. et al. Forward-genetics analysis of sleep in randomly mutagenized mice. *Nature* **539**, 378–383 (2016).
13. Saper, C. B. & Fuller, P. M. Wake-sleep circuitry: an overview. *Curr. Opin. Neurobiol.* **44**, 186–192 (2017).
14. Liu, S., Liu, Q., Tabuchi, M. & Wu, M. N. Sleep drive is encoded by neural plastic changes in a dedicated circuit. *Cell* **165**, 1347–1360 (2016).
15. Lizcano, J. M. et al. LKB1 is a master kinase that activates 13 kinases of the AMPK subfamily, including MARK/PAR-1. *EMBO J.* **23**, 833–843 (2004).
16. Erickson, B. K. et al. Evaluating multiplexed quantitative phosphopeptide analysis on a hybrid quadrupole mass filter/linear ion trap/orbitrap mass spectrometer. *Anal. Chem.* **87**, 1241–1249 (2015).
17. McAlister, G. C. et al. MultiNotch MS3 enables accurate, sensitive, and multiplexed detection of differential expression across cancer cell line proteomes. *Anal. Chem.* **86**, 7150–7158 (2014).
18. Weekes, M. P. et al. Quantitative temporal viromics: an approach to investigate host-pathogen interaction. *Cell* **157**, 1460–1472 (2014).
19. Paulo, J. A. et al. Effects of MEK inhibitors GSK1120212 and PD0325901 in vivo using 10-plex quantitative proteomics and phosphoproteomics. *Proteomics* **15**, 462–473 (2015).
20. Humphrey, S. J., James, D. E. & Mann, M. Protein phosphorylation: a major switch mechanism for metabolic regulation. *Trends Endocrinol. Metab.* **26**, 676–687 (2015).
21. Greengard, P., Valtorta, F., Czernik, A. J. & Benfenati, F. Synaptic vesicle phosphoproteins and regulation of synaptic function. *Science* **259**, 780–785 (1993).
22. Cesca, F., Baldelli, P., Valtorta, F. & Benfenati, F. The synapsins: key actors of synapse function and plasticity. *Prog. Neurobiol.* **91**, 313–348 (2010).
23. Cantrell, A. R. et al. Molecular mechanism of convergent regulation of brain Na+ channels by protein kinase C and protein kinase A anchored to AKAP-15. *Mol. Cell. Neurosci.* **21**, 63–80 (2002).
24. Tatsuki, F. et al. Involvement of Ca2+-dependent hyperpolarization in sleep duration in mammals. *Neuron* **90**, 70–85 (2016).
25. Campbell, I. G. & Feinberg, I. NREM delta stimulation following MK-801 is a response of sleep systems. *J. Neurophysiol.* **76**, 3714–3720 (1996).
26. Campbell, I. G. & Feinberg, I. Noncompetitive NMDA channel blockade during waking intensely stimulates NREM delta. *J. Pharmacol. Exp. Ther.* **276**, 737–742 (1996).
27. Schaffer, B. E. et al. Identification of AMPK phosphorylation sites reveals a network of proteins involved in cell invasion and facilitates large-scale substrate prediction. *Cell Metab.* **22**, 907–921 (2015).
28. Clark, K. et al. Phosphorylation of CRTC3 by the salt-inducible kinases controls the interconversion of classically activated and regulatory macrophages. *Proc. Natl Acad. Sci. USA* **109**, 16986–16991 (2012).

METHODS

General materials. Tandem mass tag (TMT) isobaric reagents, water and organic solvents were purchased from Thermo Fisher Scientific. Titansphere titanium dioxide (TiO_2) beads were from GL Sciences. Phospho-tag was from Wako Pure Chemical Industries. Unless otherwise noted, all other chemicals were from Sigma-Aldrich or Nacalai Tesque.

Animal studies. All animal experiments were performed according to procedures approved by the Institutional Animal Care and Use Committee of University of Tsukuba or University of Texas Southwestern Medical Center at Dallas. All mice used were males on a C57BL/6N background and were housed under humidity- and temperature-controlled conditions ($22–25 \pm 1\,°C$) on a 12-h light–dark cycle. Food and water were provided ad libitum.

Sleep phenotype analysis. The sleep–wake behaviours were analysed as previously described with modifications[12]. Electroencephalogram (EEG)/electromyogram (EMG) data were visualized and analysed using a custom semi-automated staging MatLab (MathWorks)-based program, followed by visual inspection. We did not apply blinding and only excluded animals with unreadable EEG signals from final sleep analysis. In brief, mice were implanted with the EEG/EMG electrodes at the age of 8–10 weeks, and EEG/EMG signals were recorded during weeks 12–20. Age-matched control and treatment groups of animals were used for each experiment. Following semi-automated analysis of EEG/EMG data, EEG signals were subjected to fast Fourier transform analysis for 1 to 30 Hz with 1-Hz bins. Wake was defined by low amplitude, fast EEG and high amplitude, variable EMG; NREMS by high amplitude, delta (1–4 Hz) frequency EEG and low EMG tonus; and REMS by dominant theta (6–9 Hz) frequency EEG and EMG atonia. Absolute and relative power spectrum analyses of corresponding states within indicated ZT times were performed; for relative power spectrum analysis (%), the EEG power of each frequency bin was expressed as a percentage of the total power over all frequency bins (1–30 Hz). Absolute NREMS delta power density (arbitrary units) is determined by the delta band of NREMS and normalized to the average NREMS delta power during ZT8 to ZT11 of the baseline recording day[10]; relative delta power density (%) is defined by the ratio of delta power (1–4 Hz) to total power of NREMS EEG. In circadian variation plots, each data point represents the mean value of NREMS delta power or duration in the following 1 h.

Experimental design. To examine how different treatments affect sleep/wake behaviours, 3-day baseline EEG/EMG recordings were conducted after mice were acclimated for a week. Mice remained in the same recording chamber for a 3–6-day interval between treatments. No abnormal EEG/EMG signals were confirmed during the interval before next treatment.

For the sleep deprivation model, mice were sleep deprived on an automated orbital shaker with access to food and water[12]. A 1-day baseline recording taken before sleep deprivation was used as the basal condition. Whole brains or livers were collected at ZT6 for ad libitum sleep (S6) and sleep-deprived (SD6, ZT0–ZT6) wild-type mice, or at ZT9 for 6-h sleep deprivation followed by 3-h recovery sleep (RS3) wild-type mice. For time-course sleep-deprivation, whole brains of wild-type mice were collected at ZT0 (SD0) or after 1, 3 or 6 h of sleep deprivation (SD1, SD3, SD6). For the *Sleepy* model, baseline EEG/EMG recording data were used; whole brains were collected for $Sik3^{+/+}$ (wild-type) and $Sik3^{Slp/+}$ (*Sleepy*) at ZT12.5. For food/water deprivation experiments, sham deprived (old food/water exchanged for new food/water) and deprived (all food/water removed at indicated ZT) were conducted in both normal sleep and sleep-deprived conditions; whole brains were collected at ZT6 for both conditions. For MK801 treatment, we performed intraperitoneal injection of mice with vehicle (0.9% saline) followed by 2 mg/kg MK801 (Sigma-Aldrich). Wild-type mice were injected at ZT17 in the previous dark phase followed by EEG/EMG recording at the onset of light phase (ZT0); whole brains were collected at ZT23.5, 6.5 h after MK801 administration. For HG-9-91-01[28] (ApexBio) treatment, we performed intracerebroventricular injection of mice with vehicle (3% DMSO) followed by 8 mg/kg HG-9-91-01. $Sik3^{Slp/+}$ mice were injected at ZT6 and ZT9; whole brains were collected at ZT11.5. Wild-type mice were injected at ZT0 and ZT3 during sleep deprivation (ZT0–ZT6) whole brains were collected at ZT6. The organization of sleep experiments and sleep phenotype results are listed in Supplementary Table 7b.

Tissue lysate preparation. Mouse tissues (whole brain or liver) were quickly dissected at indicated ZT, rinsed with PBS and flash frozen in liquid nitrogen. Typically, one mouse brain was homogenized in a glass tissue homogenizer with 5 ml of lysis buffer (50 mM HEPES, pH 7.4, 150 mM NaCl, 2.5% SDS, 2 mM $MgCl_2$) freshly supplemented with protease and phosphatase inhibitor cocktail tablets (Roche). Tissue homogenates were incubated at room temperature for 30 min and centrifuged at $15,000g$ for 20 min. The supernatant was carefully transferred to a new tube without disturbing the pellet. Protein concentration of protein lysates was determined using the bicinchoninic acid (BCA) assay (Thermo Scientific Pierce).

For comparison of the SIK3 and SLEEPY interactomes, wild-type, Flag-HA-$Sik3^+$ and Flag-HA-$Sik3^{Slp}$ knock-in mouse brains were lysed in ice-cold lysis buffer (20 mM HEPES, pH 7.4, 150 mM NaCl, 1 mM EDTA, 1% Triton X-100,

2 mM $MgCl_2$, 15 mM NaF, 10 mM $Na_4P_2O_7$) freshly supplemented with protease/phosphatase inhibitors in a glass tissue homogenizer[12]. After 30 min incubation on ice, brain homogenates were centrifuged at $13,000g$ for 20 min at 4 °C. The supernatant was pre-cleared with IgG and Protein G beads for 30 min before immunoprecipitation. 50 μl of anti-Flag antibody-conjugated Sepharose beads (A2220, Sigma-Aldrich) was added to each pre-cleared lysate and rotated overnight at 4 °C. The beads were washed five times with cold wash buffer (20 mM HEPES, pH 7.4, 150 mM NaCl, 1 mM EDTA, 1% Triton X-100, 2 mM $MgCl_2$, 15 mM NaF, 10 mM $Na_4P_2O_7$), 50 μl of elution buffer (2% SDS, 60 mM Tris-HCl, pH 6.8, 50 mM dithiothreitol (DTT), 10% glycerol) was then added and rotated for 10 min at 4 °C. Protein elution was repeated twice and combined into one eluate, then analysed by mass spectrometry and western blotting.

Mass spectrometry sample preparation. Protein lysate sample was reduced with DTT and then alkylated with iodoacetamide. Chloroform–methanol precipitation of protein lysate was performed, and the precipitate was resuspended in 8 M urea buffer. Protein lysate was digested for 2 h with Lys-C (1:100, enzyme to protein; Wako), followed by dilution to 2 M urea with 25 mM ammonium carbonate buffer (pH 7.8), and trypsin (1:100, enzyme to protein; Thermo Scientific Pierce) digestion overnight at room temperature. After stopping the digestion with 1% formic acid, the peptide mixture was subjected to C18 solid-phase extraction (Sep-Pak, Waters) for desalting, and subsequently vacuum-centrifuged to near-dryness.

For phosphopeptide enrichment, desalted peptides were resuspended in 1 ml phosphopeptide binding buffer (2 M lactic acid/50% acetonitrile (ACN)) and centrifuged at $15,000g$ for 20 min at room temperature. The supernatant was carefully transferred to a new tube without disturbing the pellet. TiO_2 beads were washed three times with phosphopeptide binding buffer, added to the supernatant (peptide mixture) and incubated with gentle rotation for 1 h at room temperature. Afterwards, TiO_2 beads were washed twice with phosphopeptide binding buffer and twice with wash buffer (50% ACN/0.1% trifluoroacetic acid). Phosphopeptides were eluted twice from TiO_2 beads with 500 μl elution buffer (50 mM K_2HPO_4, pH 10), acidified with 20% formic acid, subjected to desalting and vacuum-centrifuged to near-dryness.

Desalted peptides were resuspended in 200 mM HEPES (pH 8.5) and peptide concentration was determined using the BCA assay. Approximately 50 μg of peptides for each sample were labelled with TMT reagent for 1 h at room temperature. After the reaction was quenched with hydroxylamine, all TMT-labelled samples for one experiment were combined into one mixture, acidified with 20% formic acid, desalted and vacuum-centrifuged to near-dryness. The TMT-labelled sample mixture was solubilized in HPLC buffer A (1% ACN, 10 mM ammonium bicarbonate, pH 8.0) for HPLC fractionation using an Agilent 300 Extend C18 column (5-μm particles, 4.6-mm internal diameter, 150 mm in length). Different HPLC fractions were acidified with 20% formic acid and vacuum centrifuged to near-dryness. Each fraction was desalted using a StageTip, dried by vacuum centrifugation and re-suspended for LC/MS analysis.

Mass spectrometry data acquisition. Data were collected using the Orbitrap-Fusion mass spectrometry platform coupled with EASY-nLC 1000 liquid chromatography pump (Thermo Fisher Scientific). A pre-column (Acclaim PepMap 100 C18, Thermo Fisher Scientific) and analytical column (NTCC-360/75-3-125, NIKKYO) were used for sample trapping and analytical separation. Peptides were separated at a flow rate of 300 nl/min using a gradient of 6–27% ACN (0.1% formic acid) over 190 min.

The MultiNotch synchronous precursor selection MS^3-based TMT method was used on an Orbitrap-Fusion mass spectrometer using Xcalibur (v.3.0; Thermo Fisher Scientific) as described with modifications[16–19]. In brief, first stage of mass spectrum data between 400–1500 m/z were acquired from the Orbitrap at 120,000 resolution in profile data type with 4e5 AGC target, 50-ms maximum injection time. Ions were isolated in top speed mode using the quadrupole with a 0.7-m/z isolation window. MS^2 scans between 400–1200 m/z were acquired from the ion trap in centroid data type with CID fragmentation (35% collision energy) in Turbo mode, 1e4 AGC target, 50-ms maximum injection time. Top ten MS^2 fragment ions were selected using synchronous precursor selection mode for TMT reporter ions quantitation. MS^3 scans were acquired from the Orbitrap at 60,000 resolution in profile data type with HCD fragmentation (65% collision energy), 1e5 AGC target, 120-ms maximum injection time. Ions were not accumulated for all parallelisable time.

Mass spectrometry data analysis. Raw mass spectrometry files from the entire study were searched against a composite target/decoy database using SEQUEST[29–31] from Proteome Discoverer software (PD, v.2.1, Thermo Fisher Scientific). The target mouse protein database was generated from UniProt, combining all Swiss-Prot and TrEMBL entries (17 October 2015). MS^2 spectra were searched with ± 20 ppm for precursor ion mass tolerance, ± 1 Da for fragment ion mass tolerance, fully tryptic restriction, four maximal missed cleavages, dynamic mass shift for oxidation of methionine (+15.9949 Da), fixed TMT modifications on the N terminus and lysine (+229.1629 Da), and carbamidomethylation of

cysteine residues (+57.0215 Da). For phosphoproteomic analysis, additional dynamic modifications on serine, threonine and tyrosine (+79.9663 Da) were used. The peptide spectrum matches (PSMs) were filtered by Percolator[32] (PD 2.1) to achieve 1% protein and peptide FDR (according to Q value) for proteome and phosphoproteome, respectively. ptmRS[33] (PD 2.1) was used for phosphorylation site localization, which derived a localization probability score for each putatively modified site based on the given MS[2] data. Phosphopeptides with phosphorylation site probability score ≥ 25 were considered in following analysis.

TMT reporter ion signal-to-noise (S/N) values were quantified from MS[3] scans using an integration tolerance of 20 ppm (Orbitrap) with the most confident centroid setting (PD 2.1) for matching peptides. For interactome analysis, raw reporter ion abundance was used for further analysis. For proteomic and phosphoproteomic analysis, the sum of raw reporter ion for each channel was normalized assuming equal input loading of all channels. The sum of reporter ions for each protein was used in protein quantitation. The normalized quantification data of all quantified proteins, peptides or phosphopeptides were used for further analysis.

To evaluate the confidence of protein identification and quantification by PD, we used a recently developed proteomics pipeline JUMP[34,35] (v.1.12.1) to re-process one set of proteome data (EX4, SlpWTpa2) with the above same database search and PSM filtering parameters. The consistency of protein quantification between these two pipelines was indicated by Pearson correlation, which was calculated for each PSM from proteins quantified by both pipelines.

Proteomic data processing. For proteomic analysis, different isoforms were considered as different proteins for data analysis unless otherwise stated. For phosphoproteomic analysis, phosphopeptide was used for further analysis including unique and composite (containing ≥ 2 phosphorylation sites) forms. The normalized quantification data of all quantified proteins, peptides or phosphopeptides were consolidated (sum of value) to generate a unique subject ID. The consolidated abundance values were then scaled for each protein or phosphopeptide so that the average abundance was one. The scaled data from different TMT-multiplex experiments for the same comparison (for example, *Sleepy*/wild-type group) were integrated together based on unique subject ID. The multiple unpaired t-test (P value) analysis followed by the two-stage step-up FDR (Q value) approach was used to determine statistical significance ($Q < 0.2$) for each comparison[36]. The mean value for each experiment condition was used to generate the $\log_2$(fold change) value for each unique subject, which was used for further analysis. To evaluate phosphorylation stoichiometry[37], phosphoproteome normalization was performed for SD6/RS3, SD6/S6 and *Sleepy*/wild-type groups for which whole proteome and phosphoproteome data were available. In brief, the scaled phosphopeptide abundances of SD6 and Slp groups were adjusted with the mean abundance fold-change value of corresponding protein. Pearson correlation of $\log_2$(fold change) value between normalized and un-normalized was performed to evaluate the normalization effect. The full description and datasets for all proteomic experiments are listed in Supplementary Table 1, and those for all phosphoproteomics experiments are listed in Supplementary Table 2.

For SIK3 and SLEEPY interactome analysis, raw abundance data of all quantified proteins were consolidated (sum of value) to generate unique subject IDs, and then normalized assuming equal SIK3/SLEEPY protein amount in all channels. Two criteria were used to define the interacting protein (ip) for SIK3 or SLEEPY: a) TMT intensity [Mean−Blank >10]; b) fold change [Mean/Blank >2]. For the SIK3 preferential interacting protein (SIK3-pip): (Mean SLEEPY−Blank)/(Mean SIK3−Blank) < 0.5; SLEEPY-pip: (Mean SLEEPY−Blank)/(Mean SIK3−Blank) > 2. SLEEPY-pip proteins were used for the Gene Ontology (GO) cellular component enrichment analysis through Gene Ontology Consortium and PANTHER classification system[38–40]. All 22,262 genes of *Mus musculus* in the database were used as reference to determine the fold enrichment. Fisher's exact with FDR multiple test correction was used to determine statistical significance. The full description and datasets are listed in Supplementary Table 6.

Protein phosphorylation-state analysis. The phosphorylation state change (ΔPs) value for individual proteins is calculated as the sum of $\log_2$(fold change) value of all phosphopeptides with statistically significant changes ($Q < 0.2$) from all protein isoforms encoded by the same gene. If none of a phosphopeptide's Q values is above 0.2, the ΔPs value will be zero. The total quantified phosphopeptides number of the SD6/RS3 group was used for the ΔPs value normalization with other comparisons of brain phosphoproteome in this study. Normalized ΔPs value was used for further analysis to determine the hyperphosphorylated or hypophosphorylated proteins. To set up the cutoff for ΔPs value, two null tests were performed using data from SD6/RS3 and *Sleepy*/wild-type phosphoproteomes, briefly, data from channels with even number between two groups were swapped to determine the FDR. For two null tests, no phosphopeptide has a Q value above 0.2 and ΔPs value is zero for all proteins (Supplementary Table 2z, aa). Because average standard deviation (s.d.) for ΔPs value of SD6/RS3, SD6/S6 and *Sleepy*/wild-type groups is 1.1 (Supplementary Table 3d), we applied a stringent cut-off for ΔPs value at ± 2.4 (>2 s.d.) for each comparison group to represent the concept of cumulative

phosphorylation. Hyperphosphorylated (hyper, ΔPs >2.4), hypophosphorylated (hypo, ΔPs <−2.4) phosphoproteins. The full description and datasets are listed in Supplementary Table 3.

As previously described[4], in the normal sleep–wake model, mouse forebrains (cortex plus hippocampus) were collected at ZT16 (W4) and ZT4 (S4) to purify PSD fractions for phosphoproteomic analysis. For analysis of the normal sleep–wake model, the raw phosphopeptide data from supplementary tables 2A (hyperphosphorylated during wake (10pm/10am ratio >1.3)) and S2B (hyperphosphorylated in the PSD during sleep (10am/10pm ratio >1.3, or 10pm/10am ratio <0.77)) in ref. 4 were combined into one data table. The raw quantification data of all phosphopeptides were consolidated (sum of value) to generate a unique subject ID and $\log_2$(fold change) value. It should be noted that no statistical test was performed for phosphopeptide comparisons as there were only two technical replicates for each condition. The ΔPs value for each protein is calculated as the sum of $\log_2$(fold change) value of all phosphopeptides from all protein isoforms encoded by the same gene, which was not normalized with SD6/RS3 group. The full description and datasets are listed in Supplementary Table 5.

Bioinformatics analysis. The sleep phenotypes, molecular and neuronal functions of 80 SNIPPs were classified manually by literature mining[23,24,41–55], the complete literature information is listed in Supplementary Table 4a. The classification of synaptic proteins was mainly based on an integrated synaptic protein database from 11 proteomics studies[56–66] as listed in Supplementary Table 4b. A protein that is shown in ≥ 2 references (Synaptic Ref Count ≥ 2) is considered as an annotated synaptic protein. To predict potential AMPK substrates, a sequence window of −5 to +4 positions around each phosphorylation site was scored with the AMPK motif analyzer[27]. Putative AMPK phosphorylation sites (score >−0.94, the score of the lowest scoring known AMPK substrate) were used for further analysis. Complete data for AMPK substrate prediction was listed in Supplementary Table 4c. Hierarchical clustering (centroid linkage with Euclidean distance) was performed with Cluster 3.0[67].

In vitro kinase assay. The kinase activities of recombinant SIK3 and SLEEPY proteins were measured by in vitro kinase assay as previously described[68]. A recombinant GST–MFF(S146) (136-RQNGQLVRNDSIVTPSPPQA-155; AMPK motif score = 1.06) fusion protein was used as substrate. Recombinant Flag-SIK3 and Flag-SLEEPY were overexpressed in HEK 293T cells and affinity purified with anti-Flag antibody-conjugated Sepharose beads. A mock preparation from HEK293T cells transfected with empty vector was used as negative control. The same amount of recombinant kinase and substrate proteins were incubated for 20 min at 30 °C in kinase reaction buffer (50 mM HEPES, pH 7.4, 1 mM EDTA, 10 mM MgCl$_2$, 0.5 mM ATP) freshly supplemented with protease/phosphatase inhibitors. Reactions were stopped by the addition of sample loading buffer; samples were resolved by SDS–PAGE followed by western blotting or by Coomassie blue staining.

Phospho-tag SDS–PAGE and immunoblotting. Equal amounts of protein samples were resolved by phospho-tag[69] (Wako) or SDS–PAGE and transferred to PVDF membrane. Phos-tag SDS–PAGE is an electrophoresis technique capable of separating phosphorylated and non-phosphorylated forms based on phosphorylation levels, owing to binding to the phospho-tag chemical, which slows the migration of phosphorylated protein[69]. The molecular weight markers are only indicative for the non-phosphorylated forms and irrelevant for the phosphorylated forms. The Rf value of 1.0 is defined as the position of bromphenol blue dye[69].

Western blotting was performed according to standard procedures using the corresponding antibodies. Antibodies were used at the optimal concentration according to the manufacturer's instructions. Lamin A/C was measured as a loading control for the quantitative analysis of immunoblots of phosphorylation-motif antibodies. Antibodies used in this study included anti-EF2 (phospho T56/T58) (ab82981, Abcam), anti-EF2 (#2332, Cell Signaling), anti-CaMKII (phospho T286) (ab32678, Abcam), anti-CaMKII (#4436, Cell Signaling), anti-nNOS (phospho S1417) (ab5583, Abcam), anti-nNOS (ab76067, Abcam), anti-KCC2 (phospho S940) (612-401-E15, Rockland), anti-KCC2 (07-432, EMD Millipore), anti-synapsin-1 (phospho S605) (#88246, Cell Signaling), anti-synapsin-1 (sc-8295, Santa Cruz), anti-phospho-AMPK Substrate Motif (LXRXX(S*/T*)) (#5759, Cell Signaling), anti-phospho-PKC substrate motif ((K/R)XS*X(K/R)) (#6967, Cell Signaling), anti-phospho-PKA substrate motif ((K/R)(K/R)X(S*/T*)) (#9624, Cell Signaling), anti-phospho-ATM/ATR substrate motif (S*Q) (#9607, Cell Signaling), anti-phospho-AKT substrate motif (RXX(S*/T*)) (#9614, Cell Signaling), anti-phospho-PDK1 docking motif ((F/K)XX(F/Y)(S*/T*)(F/Y)) (#9634, Cell Signaling), anti-phospho-CK2 substrate motif ((S*/T*)DXE) (#8738, Cell Signaling), anti-phospho-MAPK/CDK substrate motif (PXS*P, S*PX(K/R)) (#2325, Cell Signaling), anti-phospho-CDKs substrate motif ((K/H)S*P) (#9477, Cell Signaling), anti-phospho-PLK binding motif (ST*P) (#5243, Cell Signaling), anti-phospho-Thr-Pro motif (T*P, T*PP) (#3003, Cell Signaling), anti-phospho-Thr-Pro-Glu motif (T*PE, T*P) (#3004, Cell Signaling), anti-phospho-Thr-X-Arg motif (T*X(K/R)) (#2351, Cell Signaling), anti-phospho-Tyr (Y*) (#8954,

Cell Signaling), anti-Lamin A/C (sc-6215, Santa Cruz), anti-HA (Y-11) (sc-805, Santa Cruz), anti-NMDAR1 (MAB363, EMD Millipore), anti-NMDAR2B (75–101, NeuroMab), anti-SynGAP (#5539, Cell Signaling) and anti-SIK3 C-term, a custom-generated rabbit polyclonal antibody against the C-terminal 171 amino acids of mouse SIK3.

Statistical methods. Unless otherwise noted, all experimental subjects are biological replicates and at least two independent experiments were performed. ImageJ software was used to quantify intensity of protein bands. GraphPad Prism 7 or R software was used for statistical tests. No statistical methods were used to predetermine sample size. Randomization and blinding were not used. Following one-way or two-way analysis of variance (ANOVA), Fisher's LSD test compares one mean with another mean; Tukey's test compares every mean with every other mean; Dunnett's test compares every mean to a control mean; Sidak's test compares a set of means. Repeated measures or paired test was performed for matched subject comparisons. $P < 0.05$ was considered statistically significant. The complete sample size, statistical test method and results for each comparison are reported in the figure legends and described in detail in Supplementary Table 7a.

Reporting summary. Further information on experimental design is available in the Nature Research Reporting Summary linked to this paper.

Data availability. The mass spectrometry datasets, including raw data files, search engine files, full experimental summary file and Supplementary Tables 1 and 2, have been deposited to MassIVE[70,71] with accession code MSV000081865 and to Proteome Xchange with accession code PXD008558. Source Data are provided with the online version of the paper. All other datasets generated and/or analysed in the current study are available from the corresponding author on reasonable request.

29. Eng, J. K., McCormack, A. L. & Yates, J. R. An approach to correlate tandem mass spectral data of peptides with amino acid sequences in a protein database. *J. Am. Soc. Mass Spectrom.* **5**, 976–989 (1994).
30. Peng, J., Elias, J. E., Thoreen, C. C., Licklider, L. J. & Gygi, S. P. Evaluation of multidimensional chromatography coupled with tandem mass spectrometry (LC/LC–MS/MS) for large-scale protein analysis: the yeast proteome. *J. Proteome Res.* **2**, 43–50 (2003).
31. Elias, J. E. & Gygi, S. P. Target-decoy search strategy for increased confidence in large-scale protein identifications by mass spectrometry. *Nat. Methods* **4**, 207–214 (2007).
32. Kall, L., Canterbury, J. D., Weston, J., Noble, W. S. & MacCoss, M. J. Semi-supervised learning for peptide identification from shotgun proteomics datasets. *Nat. Methods* **4**, 923–925 (2007).
33. Taus, T. et al. Universal and confident phosphorylation site localization using phosphoRS. *J. Proteome Res.* **10**, 5354–5362 (2011).
34. Wang, X. et al. JUMP: a tag-based database search tool for peptide identification with high sensitivity and accuracy. *Mol. Cell. Proteomics* **13**, 3663–3673 (2014).
35. Li, Y. et al. JUMPg: an integrative proteogenomics pipeline identifying unannotated proteins in human brain and cancer cells. *J. Proteome Res.* **15**, 2309–2320 (2016).
36. Benjamini, Y., Krieger, A. M. & Yekutieli, D. Adaptive linear step-up procedures that control the false discovery rate. *Biometrika* **93**, 491–507 (2006).
37. Wu, R. et al. Correct interpretation of comprehensive phosphorylation dynamics requires normalization by protein expression changes. *Mol. Cell. Proteomics* **10**, M111 009654 (2011).
38. Ashburner, M. et al. Gene ontology: tool for the unification of biology. *Nat. Genet.* **25**, 25–29 (2000).
39. The Gene Ontology Consortium. C. Expansion of the Gene Ontology knowledgebase and resources. *Nucleic Acids Res.* **45**, D331–D338 (2017).
40. Mi, H. et al. PANTHER version 11: expanded annotation data from Gene Ontology and Reactome pathways, and data analysis tool enhancements. *Nucleic Acids Res.* **45**, D183–D189 (2017).
41. Beacham, D., Ahn, M., Catterall, W. A. & Scheuer, T. Sites and molecular mechanisms of modulation of Na(v)1.2 channels by Fyn tyrosine kinase. *J. Neurosci.* **27**, 11543–11551 (2007).
42. James, T. F. et al. The Nav1.2 channel is regulated by GSK3. *Biochim. Biophys. Acta* **1850**, 832–844 (2015).
43. Siwek, M. E. et al. The CaV2.3 R-type voltage-gated Ca^{2+} channel in mouse sleep architecture. *Sleep* **37**, 881–892 (2014).
44. Parker, M. J. et al. De novo, heterozygous, loss-of-function mutations in SYNGAP1 cause a syndromic form of intellectual disability. *Am. J. Med. Genet. A.* **167A**, 2231–2237 (2015).
45. Carlisle, H. J. et al. Deletion of densin-180 results in abnormal behaviors associated with mental illness and reduces mGluR5 and DISC1 in the postsynaptic density fraction. *J. Neurosci.* **31**, 16194–16207 (2011).
46. Soorya, L. et al. Prospective investigation of autism and genotype–phenotype correlations in 22q13 deletion syndrome and SHANK3 deficiency. *Mol. Autism* **4**, 18 (2013).
47. Ahnaou, A., Raeymaekers, L., Steckler, T. & Drinkenburg, W. H. Relevance of the metabotropic glutamate receptor (mGluR5) in the regulation of NREM–REM sleep cycle and homeostasis: evidence from mGluR5$^{-/-}$mice. *Behav. Brain Res.* **282**, 218–226 (2015).
48. Hagebeuk, E. E., van den Bossche, R. A. & de Weerd, A. W. Respiratory and sleep disorders in female children with atypical Rett syndrome caused by mutations in the CDKL5 gene. *Dev. Med. Child Neurol.* **55**, 480–484 (2012).
49. Lonart, G., Tang, X., Simsek-Duran, F., Machida, M. & Sanford, L. D. The role of active zone protein Rab3 interacting molecule 1 alpha in the regulation of norepinephrine release, response to novelty, and sleep. *Neuroscience* **154**, 821–831 (2008).
50. Iqbal, Z. et al. Homozygous and heterozygous disruptions of ANK3: at the crossroads of neurodevelopmental and psychiatric disorders. *Hum. Mol. Genet.* **22**, 1960–1970 (2013).
51. von Stulpnagel, C. et al. SYNGAP1 mutation in focal and generalized epilepsy: a literature overview and a case report with special aspects of the EEG. *Neuropediatrics* **46**, 287–291 (2015).
52. Mangatt, M. et al. Prevalence and onset of comorbidities in the CDKL5 disorder differ from Rett syndrome. *Orphanet J. Rare Dis.* **11**, 39 (2016).
53. Fehr, S. et al. The CDKL5 disorder is an independent clinical entity associated with early-onset encephalopathy. *Eur. J. Hum. Genet.* **21**, 266–273 (2013).
54. Jiang, P. et al. A systems approach identifies networks and genes linking sleep and stress: implications for neuropsychiatric disorders. *Cell Reports* **11**, 835–848 (2015).
55. Welch, J. M. et al. Cortico-striatal synaptic defects and OCD-like behaviours in Sapap3-mutant mice. *Nature* **448**, 894–900 (2007).
56. Bayes, A. et al. Comparative study of human and mouse postsynaptic proteomes finds high compositional conservation and abundance differences for key synaptic proteins. *PLoS ONE* **7**, e46683 (2012).
57. Li, J. et al. Long-term potentiation modulates synaptic phosphorylation networks and reshapes the structure of the postsynaptic interactome. *Sci. Signal.* **9**, rs8 (2016).
58. Uezu, A. et al. Identification of an elaborate complex mediating postsynaptic inhibition. *Science* **353**, 1123–1129 (2016).
59. Gonzalez-Lozano, M. A. et al. Dynamics of the mouse brain cortical synaptic proteome during postnatal brain development. *Sci. Rep.* **6**, 35456 (2016).
60. Weingarten, J. et al. The proteome of the presynaptic active zone from mouse brain. *Mol. Cell. Neurosci.* **59**, 106–118 (2014).
61. Boyken, J. et al. Molecular profiling of synaptic vesicle docking sites reveals novel proteins but few differences between glutamatergic and GABAergic synapses. *Neuron* **78**, 285–297 (2013).
62. Abul-Husn, N. S. et al. Systems approach to explore components and interactions in the presynapse. *Proteomics* **9**, 3303–3315 (2009).
63. Biesemann, C. et al. Proteomic screening of glutamatergic mouse brain synaptosomes isolated by fluorescence activated sorting. *EMBO J.* **33**, 157–170 (2014).
64. Distler, U. et al. In-depth protein profiling of the postsynaptic density from mouse hippocampus using data-independent acquisition proteomics. *Proteomics* **14**, 2607–2613 (2014).
65. Loh, K. H. et al. Proteomic analysis of unbounded cellular compartments: synaptic clefts. *Cell* **166**, 1295-1307 (2016).
66. Nakamura, Y. et al. Proteomic characterization of inhibitory synapses using a novel pHluorin-tagged γ-aminobutyric acid receptor, type A (GABA$_A$), α2 subunit knock-in mouse. *J. Biol. Chem.* **291**, 12394–12407 (2016).
67. de Hoon, M. J., Imoto, S., Nolan, J. & Miyano, S. Open source clustering software. *Bioinformatics* **20**, 1453–1454 (2004).
68. Lee, E. E. et al. A protein kinase C phosphorylation motif in GLUT1 affects glucose transport and is mutated in GLUT1 deficiency syndrome. *Mol. Cell* **58**, 845–853 (2015).
69. Kinoshita, E., Kinoshita-Kikuta, E., Takiyama, K. & Koike, T. Phosphate-binding tag, a new tool to visualize phosphorylated proteins. *Mol. Cell. Proteomics* **5**, 749–757 (2006).
70. Vizcaino, J. A. et al. ProteomeXchange provides globally coordinated proteomics data submission and dissemination. *Nat. Biotechnol.* **32**, 223–226 (2014).
71. Deutsch, E. W. et al. The ProteomeXchange consortium in 2017: supporting the cultural change in proteomics public data deposition. *Nucleic Acids Res.* **45**, D1100–D1106 (2017).
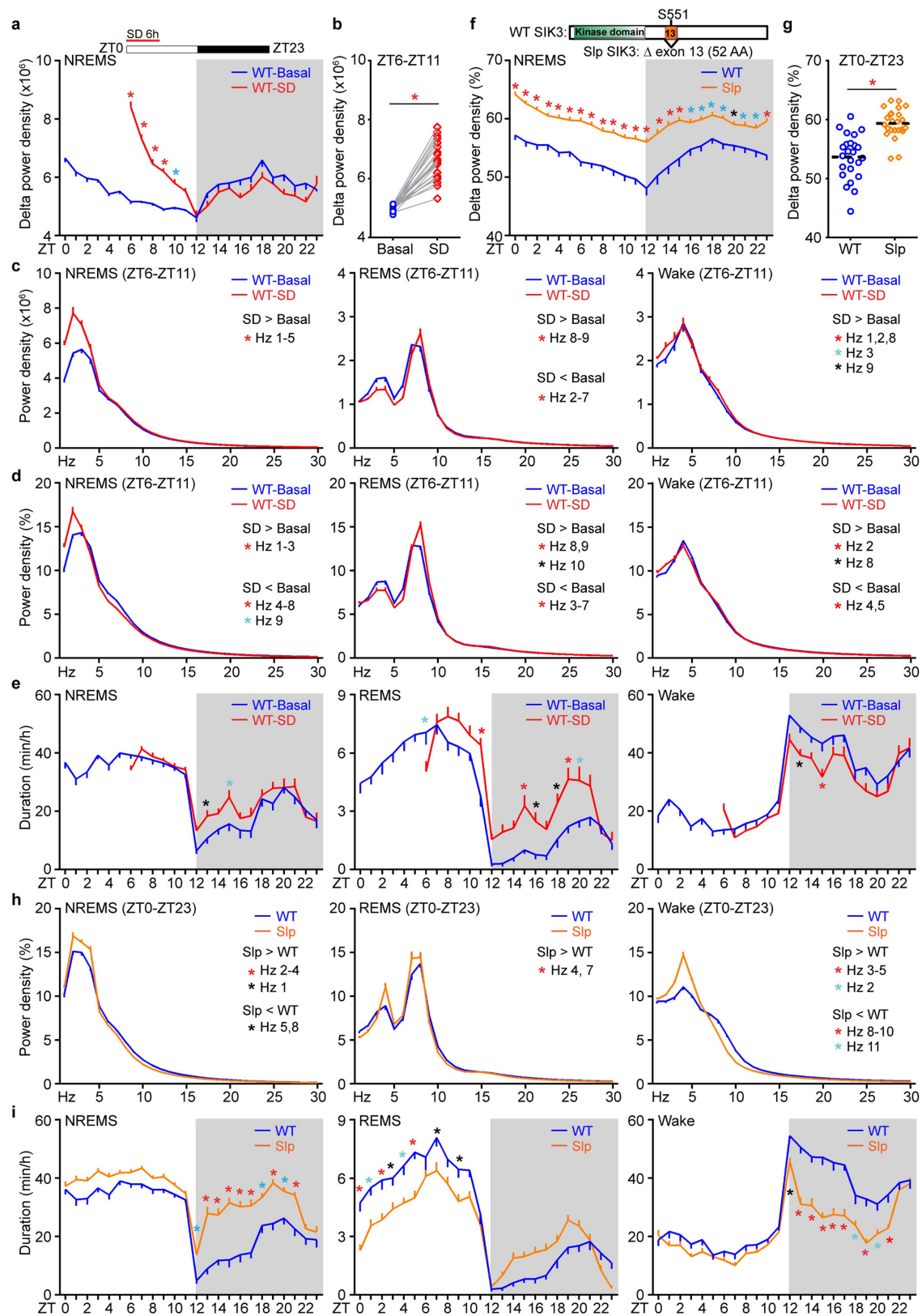
Extended Data Fig. 1 | Sleep phenotype analysis of the sleep-deprived and *Sleepy* models. a–e, Analysis of circadian (**a**) and mean (**b**) absolute NREMS delta power, absolute EEG power spectra (**c**), relative EEG power spectra (**d**) and duration (**e**) of NREMS, REMS and wake states of wild-type mice (*n* = 24) without (WT-basal) and with 6 h of sleep deprivation (WT-SD). **f–i**, Analysis of circadian (**f**) and mean (**g**) relative NREMS delta power, relative EEG power spectra (**h**) and duration (**i**) of NREMS, REMS and wake states of *Sik3*^{+/+} (WT, *n* = 24) and *Sik3*[Slp/+] (Slp, *n* = 24) mice. Mean ± s.e.m., two-way ANOVA with Sidak's test (**a**, **c–f**, **h**, **i**); Paired *t*-test, two-tailed (**b**); Mean, unpaired *t*-test, two-tailed (**g**). *(black), *P* < 0.05; *(cyan), *P* < 0.01; *(red), *P* < 0.001.
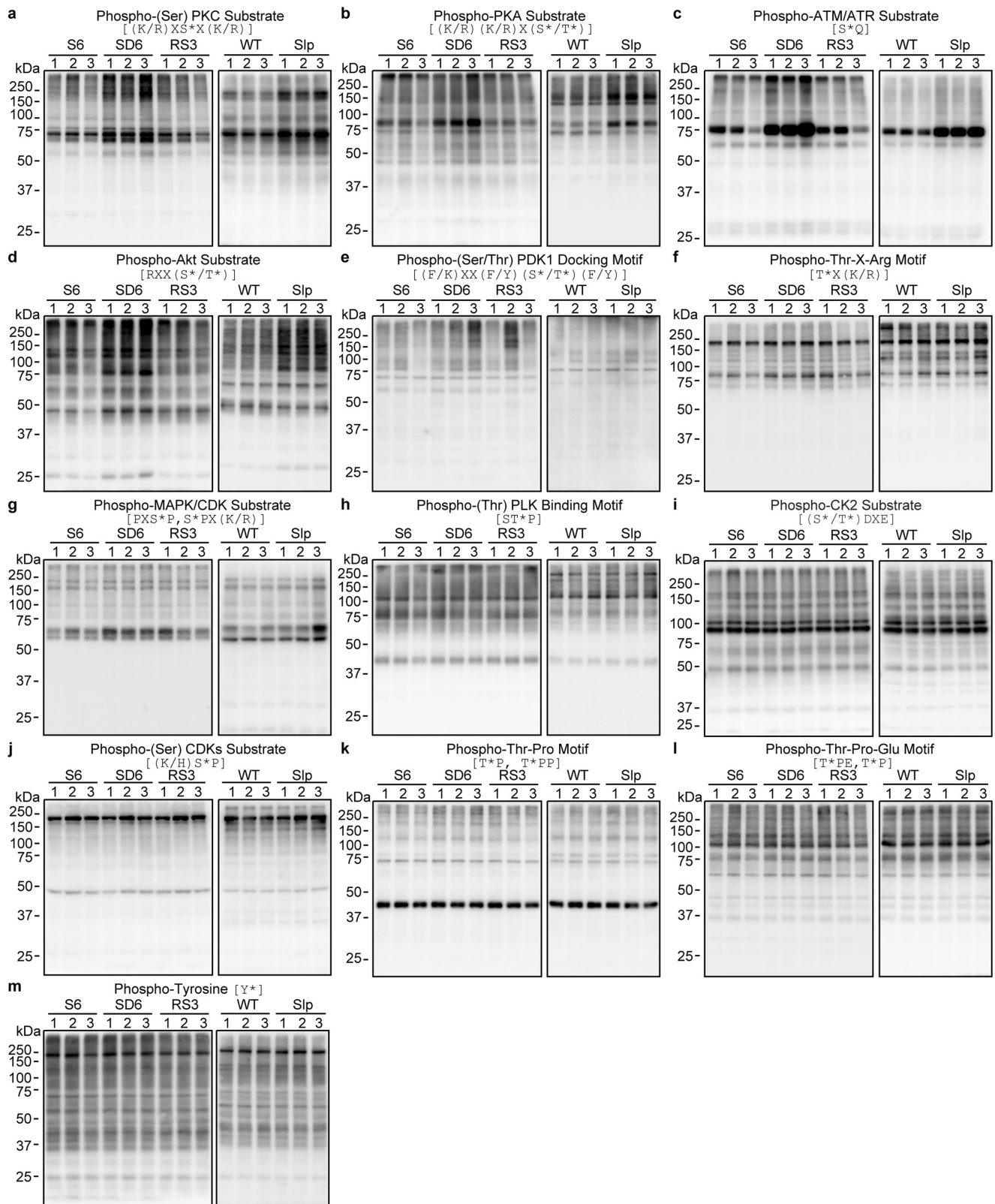
Extended Data Fig. 2 | Analysis of global signalling changes in two models of increased sleep need. a–m, Representative immunoblots using antibodies specific for 13 phosphorylation motifs to assess global signalling changes in whole brain lysates of two models. Blots represent three (sleep-deprived) or two (*Sleepy*) independent experiments. Quantitative analysis of immunoblots of all 14 phosphorylation-motif antibodies is shown in Fig. 1c. $n = 12$ (S6), 9 (SD6, RS3), 6 (wild-type, *Sleepy*).
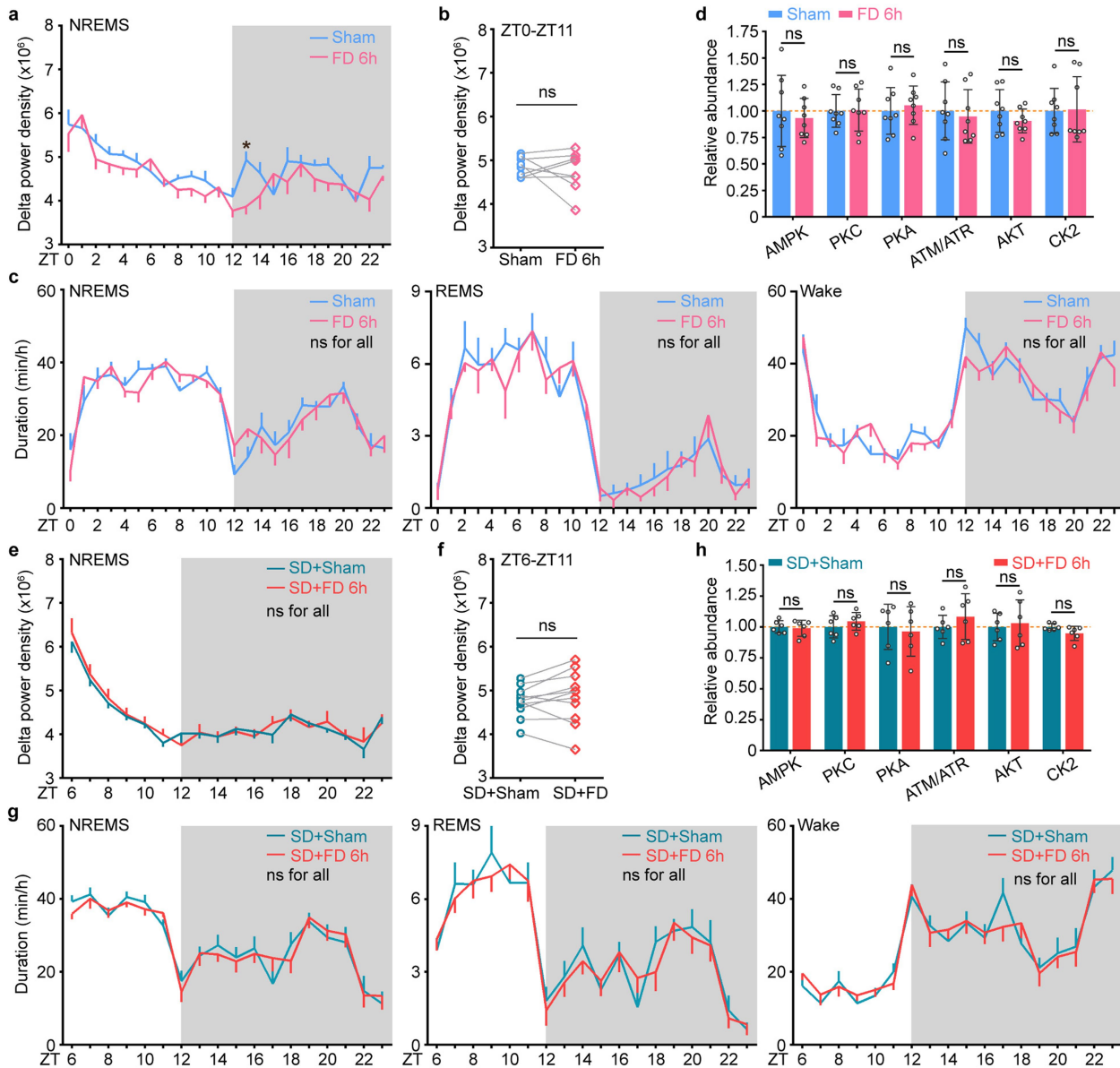
Extended Data Fig. 3 | Analysis of sleep phenotype and signalling changes after food-and-water deprivation in the baseline and sleep deprivation conditions. a–c, Analysis of circadian (**a**) and mean (**b**) absolute NREMS delta power, and duration (**c**) of NREMS, REMS and wake states, of wild-type mice ($n = 8$) without (sham) or with 6 h of food-and-water deprivation (FD 6 h). **d,** Quantitative analysis of immunoblots with six phosphorylation-motif antibodies using whole brain lysates of sham and 6-h food-and-water deprived mice ($n = 8$) collected at ZT6. **e–g,** Analysis of circadian (**e**) and mean (**f**) absolute NREMS delta power, and duration (**g**) of NREMS, REMS and wake states, of wild-type mice ($n = 11$) without (SD + sham) or with 6-h food-and-water deprivation during 6-h sleep deprivation (SD + FD 6 h). **h,** Quantitative analysis of immunoblots with six phosphorylation-motif antibodies using whole brain lysates of SD + sham and SD + FD mice ($n = 6$) collected at ZT6. Mean ± s.e.m., two-way ANOVA, Sidak's test (**a, c, e, g**); Paired t-test, two-tailed (**b, f**); Mean ± s.d., two-way ANOVA, Fisher's LSD test (**d, h**). *(black), $P < 0.05$; ns, $P > 0.05$.
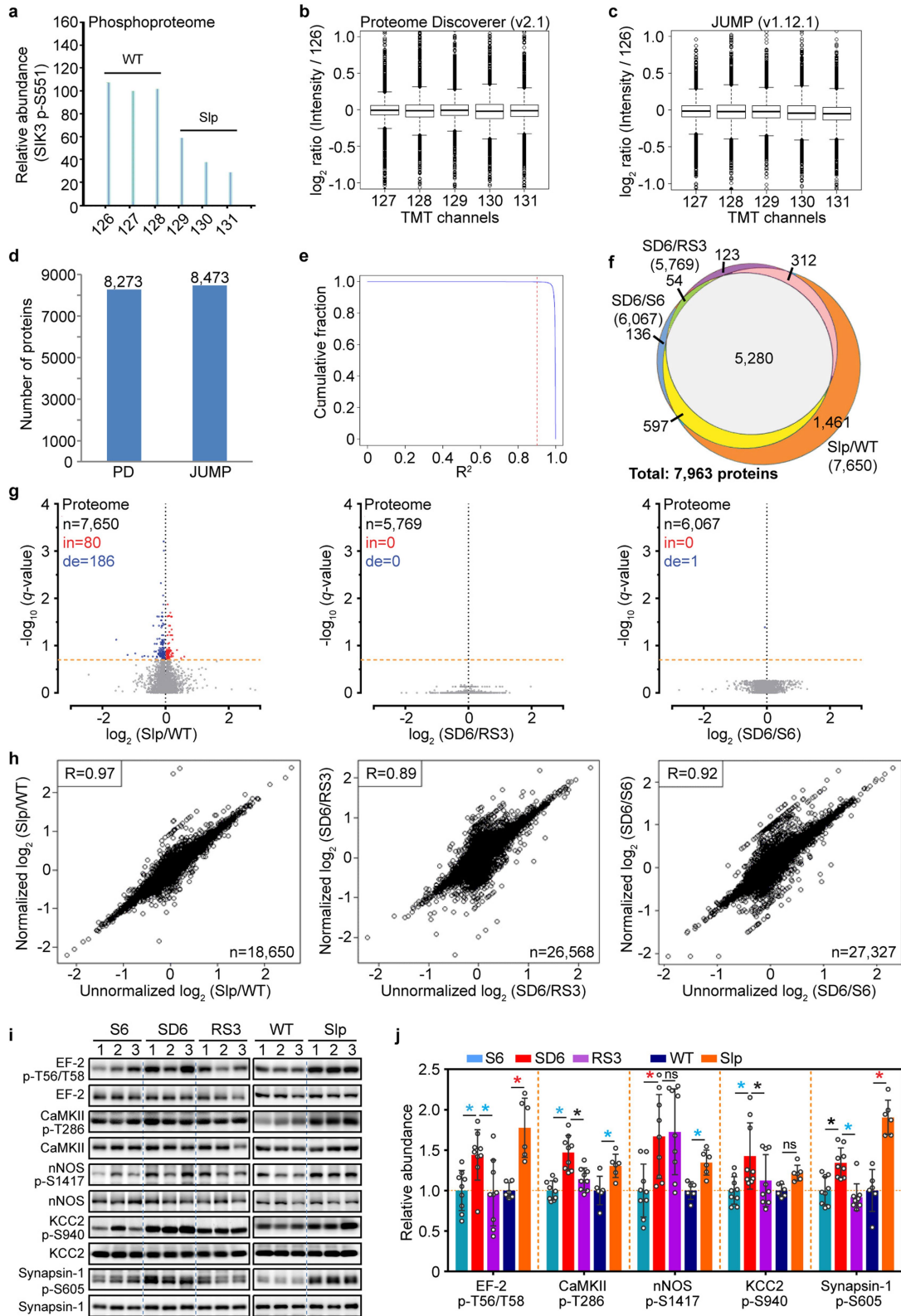
Extended Data Fig. 4 | See next page for caption.

Extended Data Fig. 4 | Quality assessment of proteomic and phosphoproteomic analysis. a, Representative TMT quantification spectrum for the pS551-containing phosphopeptide from the skipped *Sik3* exon-13 among phosphoproteomic data of the *Sleepy* model (two independent experiments). **b–e**, Quality assessment of one proteomic dataset (EX4, SlpWTpa2) by two search pipelines. Global distribution of protein quantification using Proteome Discoverer (PD v.2.1; $n = 8,273$) (**b**) and JUMP (v.1.12.1; $n = 8,473$) (**c**). Boxes correspond to the 25th, 50th and 75th percentiles of the data, whiskers extend to 1.5-fold of the interquartile range. A similar number of accepted proteins (1% FDR) were identified by two pipelines (**d**). Pearson correlation between the two pipelines was calculated for each PSM from quantified proteins by both pipelines (**e**). The vast majority (99.88%) of PSMs ($n = 73,454$) have R^2 values larger than 0.9 (red dashed line). **f**, A Venn diagram showing overlaps of quantified proteins between whole brain proteomes of *Sleepy* and sleep-deprived models. **g**, Volcano plots showing comparative analysis of *Sleepy*/wild-type, SD6/RS3 and SD6/S6 proteomes. Multiple unpaired *t*-test (*P* value) followed by FDR (*Q* value) analysis. *x* axis, $\log_2$(fold change) in abundance; *y* axis, $-\log(Q$ value) of abundance change. The numbers of total (n), increased (in: $Q < 0.2$, red) and decreased (de: $Q < 0.2$, blue) subjects are shown. Orange dotted lines indicate $Q = 0.2$. **h**, Pearson correlation between normalized and unnormalized phosphopeptides in *Sleepy*/wild-type, SD6/RS3, SD6/S6 groups. The numbers of phosphopeptides that can be normalized are shown. **i**, Immunoblots were performed with phosphorylation-site specific antibodies to verify hyper-phosphorylation of several proteins in two models. Three or two independent experiments for sleep-deprived or *Sleepy* models, respectively. **j**, Quantitative analysis of immunoblots in **i**, normalized with whole protein abundance, for *Sleepy* ($n = 6$) and sleep-deprived ($n = 9$) models. Mean ± s.d., two-way ANOVA with Fisher's LSD test. *(black), $P < 0.05$; *(cyan), $P < 0.01$; *(red), $P < 0.001$; ns, $P > 0.05$.
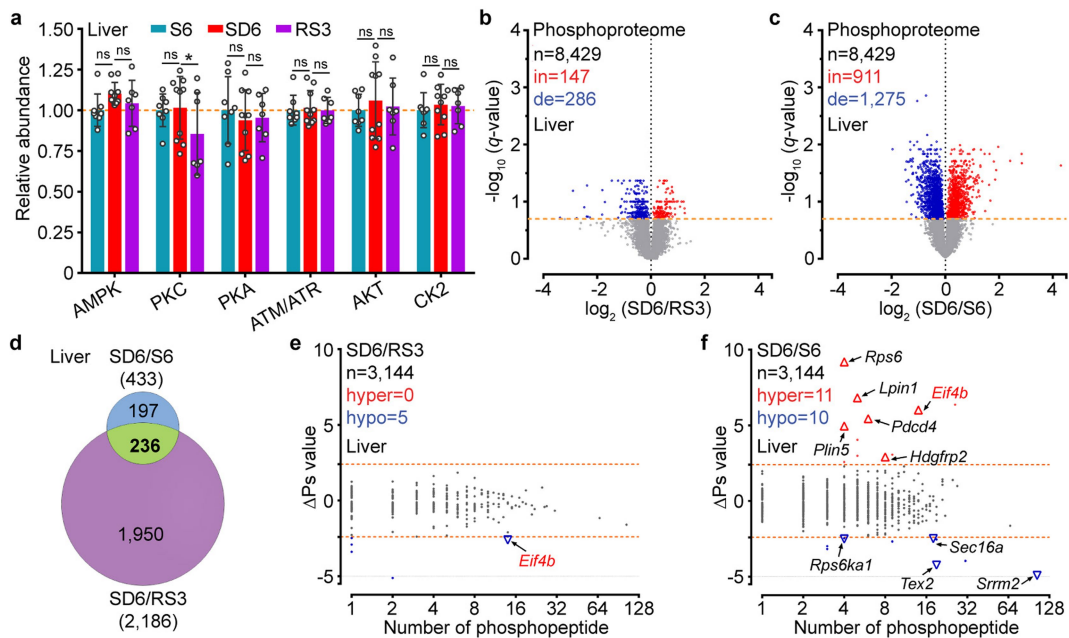
Extended Data Fig. 5 | Liver phosphoproteome analysis of the sleep-deprived model. a, Quantitative analysis of immunoblots with six phosphorylation-motif antibodies using whole liver lysates from the sleep-deprived model. $n = 8$ (S6), 10 (SD6), 7 (RS3). Mean ± s.d., two-way ANOVA with Fisher's LSD test. *(black), $P < 0.05$; ns, $P > 0.05$. **b**, **c**, Volcano plots showing comparative analysis of liver phosphoproteomes in the SD6/RS3 (**b**) and SD6/S6 (**c**) groups. Multiple unpaired t-test (P value) followed by FDR (Q value) analysis. x axis, $\log_2$(fold change) in abundance; y axis, $-\log(Q$ value) of abundance change. The numbers of total (n), increased (in: $Q < 0.2$, red) and decreased (de: $Q < 0.2$, blue) subjects are shown. Orange dotted lines indicate $Q = 0.2$. **d**, A Venn diagram showing overlaps of significantly changed ($Q < 0.2$) phosphopeptides among the SD6/RS3 and SD6/S6 groups. **e**, **f**, Global ΔPs analysis of all phosphoproteins identified in the SD6/RS3 (**e**) and SD6/S6 (**f**) groups of liver phosphoproteomes. Dotted lines, ΔPs = ±2.4.
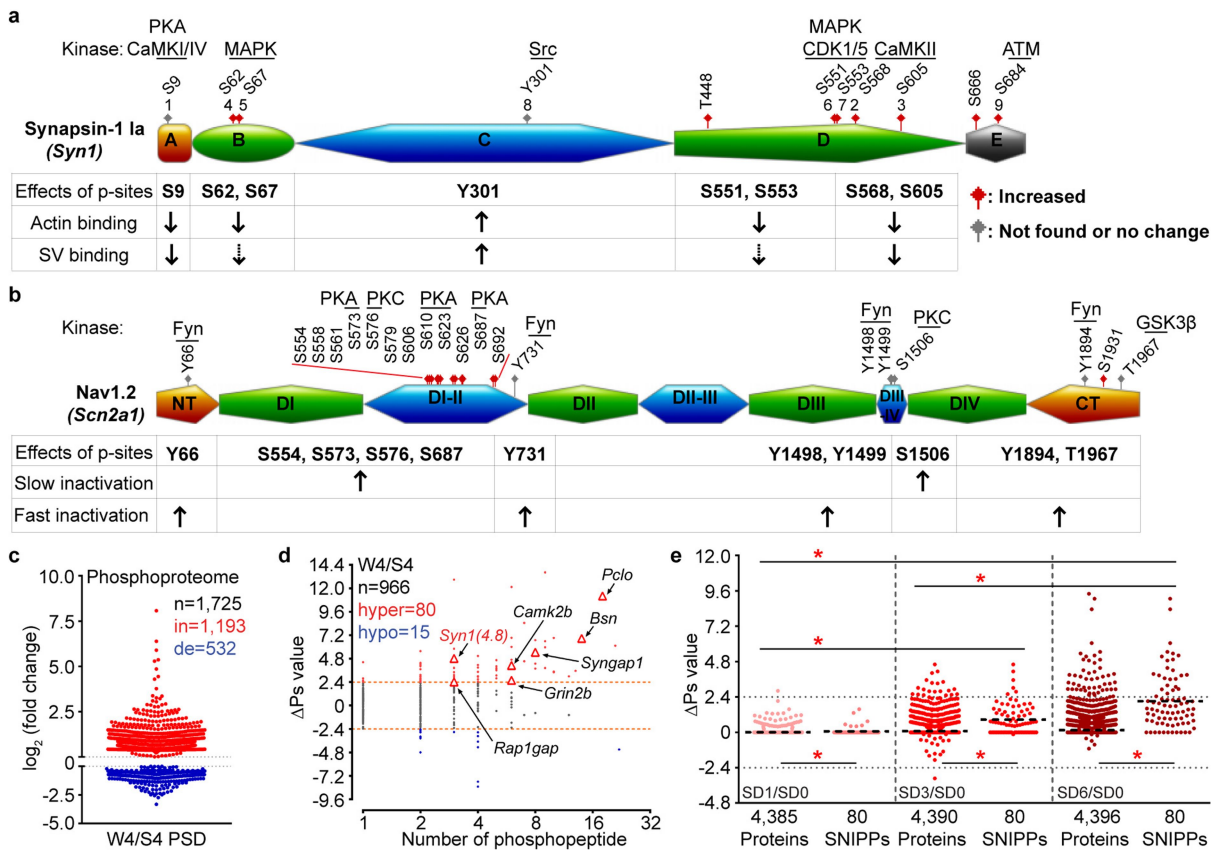
Extended Data Fig. 6 | Examples of cumulative phosphorylation of SNIPPs and synaptic phosphoproteomic analysis of normal sleep–wake model. a, b, A schematic of the domain structure of synapsin-1[22] (**a**) and Nav1.2[23,41,42] (**b**) that summarizes known phosphorylation sites, kinases and physiological functions. Synapsin-1 can be divided into five domains (domains A–E). Nav1.2 can be divided into cytoplasmic N-terminal (NT), C-terminal (CT), four homologous transmembrane domains (DI–DIV) and intracellular loops (DI–II, DII–III, DIII–IV). Amino acid numbers refer to the sequence of the mouse proteins. Sites 1–9 of synapsin-1 are designated according to the consensus in the literature. Phosphorylation sites that are undetected or unchanged in our experiments are labelled in grey, whereas those that exhibit significantly increased phosphorylation with sleep deprivation are shown in red. Dashed arrows indicate the presence of contrasting data for biological functions in the literature. **c**, Published forebrain PSD phosphoproteome results[4] were used for comparative analysis between normal wake (W4) and sleep (S4) brains. **d**, Global ΔPs analysis of all identified phosphoproteins in the W4/S4 group. Dotted lines (ΔPs = ±2.4). **e**, Quantitative ΔPs analysis of SD1/SD0, SD3/SD0 and SD6/SD0 groups. Mean; one-way ANOVA, Tukey's test (total, SNIPPs); unpaired t-test, two-tailed (total versus SNIPPs). *(red), $P < 0.001$.

a

SD6/S6 (45)

SD6/RS3 (151)

Slp/WT (190)

3

3

12

27

62

110

50

Total: 267 Hyper-Phosphoproteins
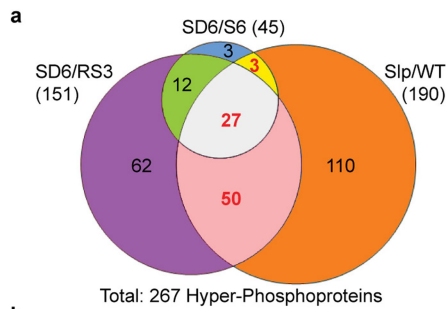
b

Action Potential

Gene	Molecular and Neuronal Functions
Scn1a	Voltage-gated Na+ channel
★ *Scn2a1*	Voltage-gated Na+ channel; Action potential backpropagation

Neurotransmitter Release

Gene	Molecular and Neuronal Functions
Arfgap3	GAPs of ARF1 for endocytosis
Brsk1	Protein kinase; AMPK-related; Short-term plasticity
★ *Bsn*	Active zone scaffolding protein; Short-term plasticity
Cacna1e	Voltage-gated Ca2+ channel
Cadps	Synaptic vesicle protein for exocytosis; Short-term plasticity
Camk2b	Protein kinase
Dmxl2	Scaffolding protein for exocytosis
★ *Dnm1*	GTPase for endocytosis; Short-term plasticity
★ *Pclo*	Active zone scaffolding protein
★ *Rims1*	Active zone protein for exocytosis; Short-term plasticity
Rims2	Active zone protein for exocytosis
★ *Syn1*	Synaptic vesicle protein; Short-term plasticity

Dendrite Morphogenesis

Gene	Molecular and Neuronal Functions
Abi1	Regulator of protein kinase ABL1
Arhgap39	GAPs of Rac1 and Cdc42
Arhgef2	GEFs of RhoA; AMPAR complex
★ *Mark2*	Protein kinase; AMPK-related
Mink1	Protein kinase; Rap2 effector
Rap1gap	GAPs of Rap1
★ *Sipa1l1*	GAPs of Rap2; PSD-95/NMDAR complex
Tanc2	PSD scaffolding protein; PSD-95 complex
Tnik	Protein kinase; Rap2 effector

Neurogenesis

Gene	Molecular and Neuronal Functions
Camsap1	Microtubule organization; Spectrin-binding
Clasp2	Microtubule dynamics; Neuronal polarity; +TIPs
Dock7	GEFs of Rac1 and Rac3; Neuronal polarity
Gprin1	Gαo binding protein; Cdc42 complex
★ *Mark1*	AMPK-related kinase; Neuronal polarity
Nav1	Microtubule dynamics; Neuronal migration; +TIPs
Rap1gap2	GAPs of Rap1; Axonogenesis
★ *Rapgef2*	GEFs of Rap and Ras; Axonogenesis
Trio	Microtubule dynamics; GEFs of Rac1 and RhoG; +TIPs

Synaptic Plasticity

Gene	Molecular and Neuronal Functions
Abl2	Protein kinase
Agap2	GAPs of ARF1 and ARF5
Ank3	Scaffolding protein
Anks1b	PSD scaffolding protein
Baiap2	Adapter protein of Cdc42; Actin reorganization
Cdkl5	Protein kinase
Cnksr2	Regulator of protein kinase RAS
Dlgap2	PSD scaffolding protein
Dlgap3	PSD scaffolding protein
Grin2b	Glutamate receptor ionotropic; NMDAR subunit
Grm5	Glutamate receptor metabotropic
Iqsec1	GEFs of ARF1 and ARF6
Iqsec2	GEFs of ARF
Lrrc7	PSD scaffolding protein
Mff	Mitochondrial fission
Plppr4	Lipid phosphatase
Rab11fip5	Rab effector; Protein trafficking
Shank2	PSD scaffolding protein
★ *Shank3*	PSD scaffolding protein
Sorbs2	Protein kinase ABL regulator
★ *Srcin1*	Protein kinase SRC regulator
Syngap1	GAPs of Ras and Rap; NMDAR complex
Synpo	Cytoskeleton organization; Actin-binding

Undetermined

| Gene	Molecular and Neuronal Functions
2010300C02Rik	Unknown
Ankrd63	Unknown
Arfgap2	GAPs of ARF1; Protein transport
Arhgap21	GAPs of RhoA and Cdc42; Golgi structure
C2cd4c	Phospholipid binding
Caskin1	Active zone scaffolding protein; CASK complex
Cep170	Microtubule organization; Centrosomal protein
Cep170b	Microtubule organization; Centrosomal protein
Clasp1	Microtubule dynamics; +TIPs
Ddx3x	RNA helicase
Ddx3y	RNA helicase
Elfn2	Regulator of protein phosphatase PP1
Exoc1	Protein exocytosis
Ildr2	ER stress; Lipid homeostasis
Map2	Microtubule stiffening
Mark4	Protein kinase; AMPK-related; Microtubule-associated
Mast1	Protein kinase; Microtubule-associated
Osbpl6	Lipid transport
Pde4b	cAMP phosphodiesterase
Pdha1	Mitochondria pyruvate dehydrogenase
Pitpnm2	Lipid PtdIns transfer
Sphkap	Regulator of protein kinase PKA
★ *Stk32c*	Protein kinase
Tbc1d10b	GAPs of Rab3A, Rab22A, Rab27A, and Rab35
Usp31	Protein deubiquitination

Extended Data Fig. 7 | Physiological functions of 80 SNIPPs. a, A Venn diagram showing overlaps of the set of hyperphosphorylated proteins (ΔPs >2.4) between sleep-deprived and *Sleepy* models. **b**, A summary of 80 SNIPPs and their physiological functions. Stars mark the 13 SWA-SNIPPs (Fig. 3f). Gene names for annotated synaptic proteins are shown in bold.
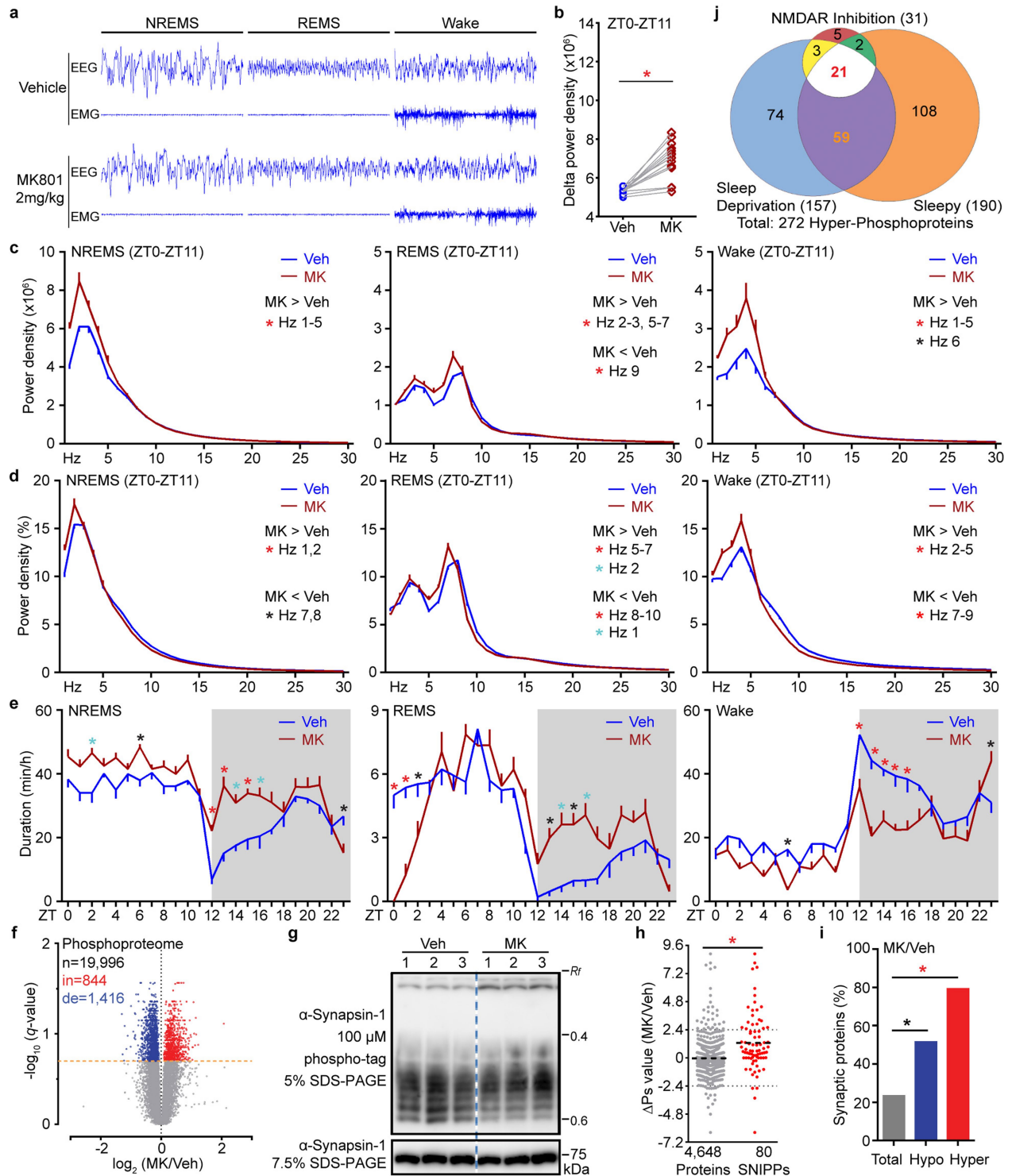
Extended Data Fig. 8 | Phosphorylation-state changes of SNIPPs correspond to changes of sleep need in NMDAR inhibition model. **a**, Representative 8-s EEG and EMG from ZT0–ZT3 for NREMS, REMS and wake for vehicle or MK801-treated mice. **b**, Mean absolute NREMS delta power analysis of vehicle or MK801-injected mice ($n = 14$). Paired t-test, two-tailed. **c**–**e**, Analysis of absolute EEG power spectra (**c**), relative EEG power spectra (**d**) and duration (**e**) for vehicle or MK801-injected wild-type mice ($n = 14$). Mean ± s.e.m., two-way ANOVA with Sidak's test. **f**, Volcano plot showing comparison between phosphoproteomes of MK801 and vehicle treated mice. Orange dotted line, $Q = 0.2$. Multiple unpaired t-test (P value) followed by FDR (Q value) analysis.

g, Phosphorylation state of synapsin-1 was assessed by SDS–PAGE followed by phospho-tag (top) and immunoblotting with anti-synapsin-1 antibody (bottom). The Rf value of 1.0 is defined as the position of bromphenol blue dye (two independent experiments). **h**, Quantitative ΔPs analysis of MK801/vehicle group. Mean, unpaired t-test, two-tailed. **i**, Percentage of synaptic proteins among the total, hypophosphorylated and hyperphosphorylated proteins in the MK801/vehicle group. χ^2 test, two-sided. **j**, Venn diagram showing overlaps of hyperphosphorylated proteins (ΔPs >2.4) among all three (*Sleepy*, SD and MK801) models. *(black), $P < 0.05$; *(cyan), $P < 0.01$; *(red), $P < 0.001$.
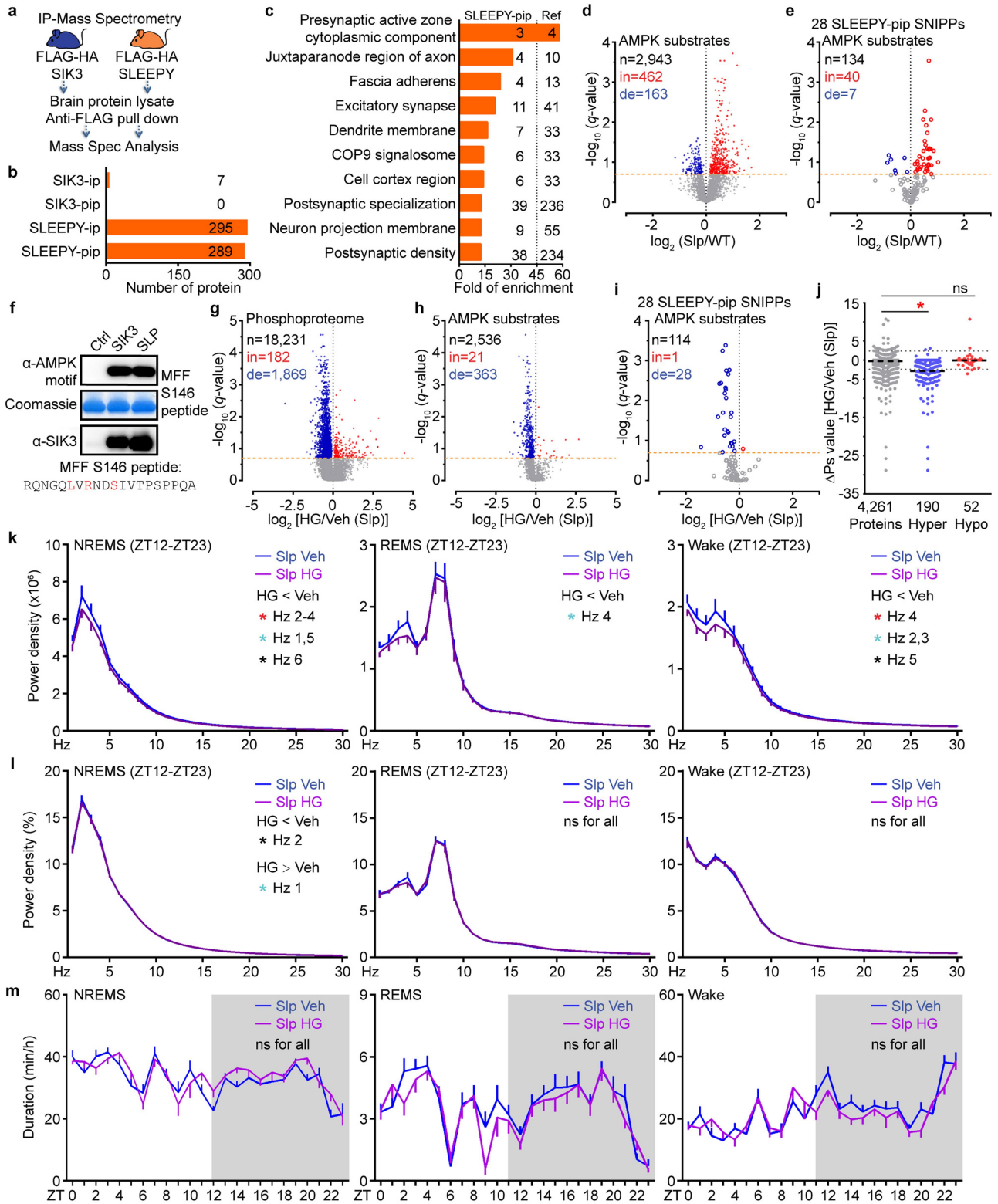
Extended Data Fig. 9 | See next page for caption.

Extended Data Fig. 9 | SLEEPY causes constitutively high sleep need by preferentially associating with and phosphorylating SNIPPs.
a, Experimental design for comparing the interactomes of SIK3 and SLEEPY from whole brain lysates. **b**, Summary of SIK3 and SLEEPY interacting proteins (ip) and preferential interacting proteins (pip). **c**, Gene-annotation enrichment analysis of 289 SLEEPY-preferential interacting proteins (SLEEPY-pip). GO cellular component enrichment analysis using all 22,262 genes of *Mus musculus* as reference (Ref). Fisher's exact with FDR multiple test correction was used to determine statistical significance. Top 10 GO terms of fold enrichment (FDR <0.0001), the gene number of SLEEPY-pip and Ref in each term are shown. **d**, **e**, Volcano plots showing phosphorylation changes of all putative AMPK substrates in the *Sleepy*/wild-type group (**d**) or from the 28 SLEEPY-pip SNIPPs (**e**). Orange dotted lines, $Q = 0.2$. **f**, In vitro kinase assay of recombinant

SLEEPY and SIK3, and immunoblotting with AMPK phosphorylation motif antibody (two independent experiments). **g–i**, Volcano plot showing comparative analysis of whole brain phosphoproteomes (**g**), all putative AMPK substrates (**h**) or from 28 SLEEPY-pip SNIPPs (**i**) in the HG/vehicle (Slp) group. Orange dotted lines, $Q = 0.2$. **j**, Quantitative ΔPs analysis of 190 hyperphosphorylated proteins and 52 hypophosphorylated proteins in the HG/vehicle (Slp) group. Dotted lines, ΔPs $= \pm 2.4$. **k–m**, Analysis of absolute EEG power spectra (**k**), relative EEG power spectra (**l**) and duration (**m**) of NREMS, REMS and wake states of $Sik3^{Slp/+}$ (Slp, $n = 14$) mice injected with vehicle (Veh) or 8 mg/kg HG at ZT6 and ZT9. Multiple unpaired t-test (P value) followed by FDR (Q value) analysis (**d**, **e**, **g–i**). Mean, one-way ANOVA with Dunnett's test (**j**). Mean $\pm$ s.e.m., two-way ANOVA with Sidak's test (**k–m**). *(black), $P < 0.05$; *(cyan), $P < 0.01$; *(red), $P < 0.001$; ns, $P > 0.05$.
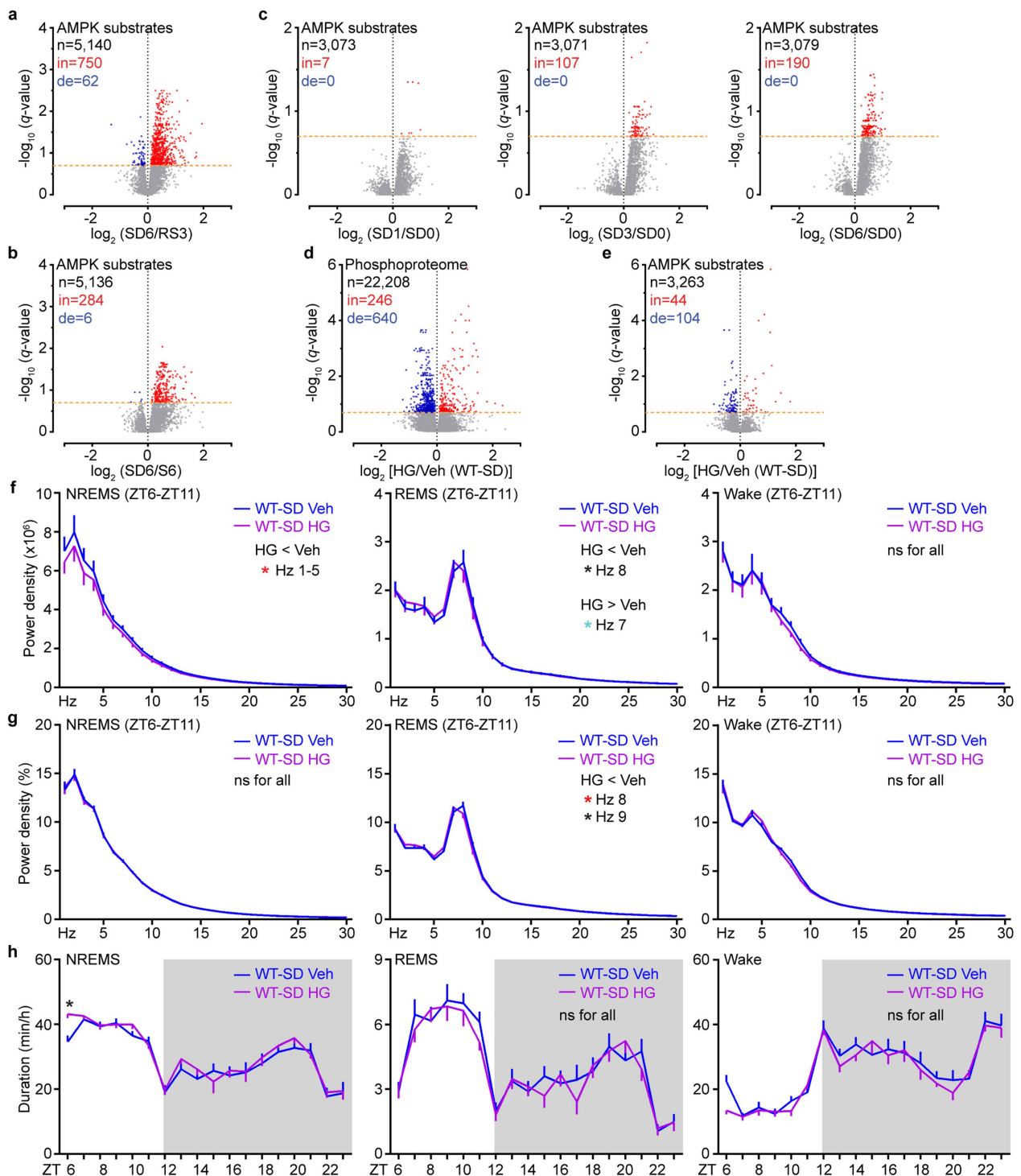
Extended Data Fig. 10 | Inhibition of SIK3 kinase activity reduces phosphorylation of AMPK substrates in sleep-deprived wild-type brains. a–c, Volcano plots showing phosphorylation changes of all putative AMPK substrates in the SD6/RS3 (**a**), SD6/S6 (**b**) and time-course sleep-deprivation groups (**c**). Orange dotted lines, Q = 0.2. **d, e**, Volcano plots showing comparative analysis of whole brain phosphoproteome (**d**) and phosphorylation changes of all putative AMPK substrates (**e**) in the HG/vehicle (WT-SD) group. Orange dotted lines, Q = 0.2. **f–h**, Analysis of absolute EEG power spectra (**f**), relative EEG power spectra (**g**) and duration (**h**) of NREMS, REMS and wake states of sleep-deprived (ZT0–ZT6) wild-type (n = 16) mice injected with vehicle (Veh) or 8 mg/kg HG at ZT0 and ZT3. Multiple unpaired t-test (P value) followed by FDR (Q value) analysis (**a–e**). Mean ± s.e.m., two-way ANOVA with Sidak's test (**f–h**). *(black), $P < 0.05$; *(cyan), $P < 0.01$; *(red), $P < 0.001$; ns, $P > 0.05$.

nature research

Corresponding author(s):   QINGHUA LIU

Reporting Summary

Nature Research wishes to improve the reproducibility of the work that we publish. This form provides structure for consistency and transparency in reporting. For further information on Nature Research policies, see Authors & Referees and the Editorial Policy Checklist.

Statistical parameters

When statistical analyses are reported, confirm that the following items are present in the relevant location (e.g. figure legend, table legend, main text, or Methods section).

n/a	Confirmed	
☐	☒	The exact sample size (*n*) for each experimental group/condition, given as a discrete number and unit of measurement
☐	☒	An indication of whether measurements were taken from distinct samples or whether the same sample was measured repeatedly
☐	☒	The statistical test(s) used AND whether they are one- or two-sided *Only common tests should be described solely by name; describe more complex techniques in the Methods section.*
☐	☒	A description of all covariates tested
☐	☒	A description of any assumptions or corrections, such as tests of normality and adjustment for multiple comparisons
☐	☒	A full description of the statistics including central tendency (e.g. means) or other basic estimates (e.g. regression coefficient) AND variation (e.g. standard deviation) or associated estimates of uncertainty (e.g. confidence intervals)
☐	☒	For null hypothesis testing, the test statistic (e.g. *F*, *t*, *r*) with confidence intervals, effect sizes, degrees of freedom and *P* value noted *Give P values as exact values whenever suitable.*
☒	☐	For Bayesian analysis, information on the choice of priors and Markov chain Monte Carlo settings
☒	☐	For hierarchical and complex designs, identification of the appropriate level for tests and full reporting of outcomes
☐	☒	Estimates of effect sizes (e.g. Cohen's *d*, Pearson's *r*), indicating how they were calculated
☐	☒	Clearly defined error bars *State explicitly what error bars represent (e.g. SD, SE, CI)*

Our web collection on statistics for biologists may be useful.

Software and code

Policy information about availability of computer code

Data collection	All raw mass spectrometry files of entire study were collected using Xcalibur (version 3.0; Thermo Fisher Scientific).
Data analysis	Mass spectrometry data (Proteome Discoverer with SEQUEST, Percolator and ptmRS , version 2.1, Thermo Fisher Scientific). Sleep data (MatLab-based custom program). Phosphorylation site score (AMPK Motif Analyzer). Hierarchical clustering (Cluster 3.0). Quantify protein band (Image J). Statistical analysis (GraphPad Prism 7 or R).

For manuscripts utilizing custom algorithms or software that are central to the research but not yet described in published literature, software must be made available to editors/reviewers upon request. We strongly encourage code deposition in a community repository (e.g. GitHub). See the Nature Research guidelines for submitting code & software for further information.

Data

Policy information about availability of data

All manuscripts must include a data availability statement. This statement should provide the following information, where applicable:

- Accession codes, unique identifiers, or web links for publicly available datasets
- A list of figures that have associated raw data
- A description of any restrictions on data availability

The mass spectrometry datasets have been deposited to MassIVE (MSV000081865). Source data are provided with the online version of the paper. All other datasets generated and/or analyzed in the current study will be available from the corresponding author on reasonable request.

Field-specific reporting

Please select the best fit for your research. If you are not sure, read the appropriate sections before making your selection.

☒ Life sciences ☐ Behavioural & social sciences ☐ Ecological, evolutionary & environmental sciences

For a reference copy of the document with all sections, see nature.com/authors/policies/ReportingSummary-flat.pdf

Life sciences study design

All studies must disclose on these points even when the disclosure is negative.

Sample size	No statistical methods were used to predetermine sample size. Required sample sizes were estimated based on the sufficient statistics and similar experiments before.
Data exclusions	SDpho1/S6-3 and SDpho2/S6-6 were not used for following analysis due to insufficient TMT labeling. Reported in Supplementary Table 2 Experiment descriptions sheet. We only exclude animals with unreadable EEG signals from final sleep analysis. Exclusion data do not affect experimental findings. Reported in Methods section.
Replication	The experimental findings were reliably reproduced. Replication of each experiments reported in Methods and fully described in Supplementary Table 1, 2, 6 and 7a.
Randomization	Same aged mice were randomly allocated into treated and control groups based on experimental design.
Blinding	A semi-automated staging MatLab-based program for EEG/EMG analysis, followed by visual inspection of observer. Blinding were not applied for EEG/EMG analysis. To further ensure sufficient statistics and valid results, we repeat every experiment at least twice, with n=4-8 mice for each EEG recording experiment. For pharmacological experiments, such as HG treatments, we will not only repeat the same experiment at least twice with independent animal groups, but also repeat drug treatment twice for the same animal groups to ensure that our observations are reproducible.

Reporting for specific materials, systems and methods

Materials & experimental systems

n/a	Involved in the study
☒	☐ Unique biological materials
☐	☒ Antibodies
☒	☐ Eukaryotic cell lines
☒	☐ Palaeontology
☐	☒ Animals and other organisms
☒	☐ Human research participants

Methods

n/a	Involved in the study
☒	☐ ChIP-seq
☒	☐ Flow cytometry
☒	☐ MRI-based neuroimaging

Antibodies

Antibodies used	Antibodies used in this study included anti-EF2 (phospho T56/T58) [ab82981, Abcam], anti-EF2 [#2332, Cell Signaling], anti-CaMKII (phospho T286) [ab32678, Abcam], anti-CaMKII [#4436, Cell Signaling], anti-nNOS (phospho S1417) [ab5583, Abcam], anti-nNOS [ab76067, Abcam], anti-KCC2 (S940) [612-401-E15, Rockland], anti-KCC2 [07-432, EMD Millipore], anti-Synapsin-1 (Ser605) [#88246, Cell Signaling], anti-Synapsin-1[sc-8295, Santa Cruz], anti-Phospho-AMPK Substrate Motif [LXRXX(S*/T*)]

[#5759, Cell Signaling], anti-Phospho-PKC Substrate Motif [(K/R)XS*X(K/R)] [#6967, Cell Signaling], anti-Phospho-PKA Substrate Motif [(K/R)(K/R)X(S*/T*)] [#9624, Cell Signaling], anti-Phospho-ATM/ATR Substrate Motif [S*Q] [#9607, Cell Signaling], anti-Phospho-Akt Substrate Motif [RXX(S*/T*)] [#9614, Cell Signaling], anti-Phospho-PDK1 Docking Motif [(F/K)XX(F/Y)(S*/T*)(F/Y)] [#9634, Cell Signaling], anti-Phospho-CK2 Substrate Motif [(S*/T*)DXE] [#8738, Cell Signaling], anti-Phospho-MAPK/CDK Substrate Motif [PXS*P, S*PX(K/R)] [#2325, Cell Signaling], anti-Phospho-CDKs Substrate Motif [(K/H)S*P] [#9477, Cell Signaling], anti-Phospho-PLK Binding Motif [ST*P] [#5243, Cell Signaling], anti-Phospho-Thr-Pro Motif [T*P, T*PP] [#3003, Cell Signaling], anti-Phospho-Thr-Pro-Glu Motif [T*PE, T*P] [#3004, Cell Signaling], anti-Phospho-Thr-X-Arg Motif [T*X(K/R)] [#2351, Cell Signaling], anti-Phospho-Tyrosine [Y*] [#8954, Cell Signaling], anti-Lamin A/C [sc-6215, Santa Cruz], anti-HA (Y-11) [sc-805, Santa Cruz], anti-NMDAR1 [MAB363, EMD Millipore], anti-NMDAR2B [75-101, NeuroMab], anti-SynGAP [#5539, Cell Signaling], and anti-SIK3 C-term [a custom generated rabbit polyclonal antibody against the C-terminal 171 amino acids of mouse SIK3].

Validation	The custom generated anti-SIK3 C-term antibody has been used in Funato et al., Nature, 2016. The validation information of all commercial antibodies used in this study can be found on the manufacturer's websites. Western blotting was performed according to standard procedures using the corresponding antibodies. Dilution of antibodies at the optimal concentration was used according to the manufacturer's instructions.

Animals and other organisms

Policy information about studies involving animals; ARRIVE guidelines recommended for reporting animal research

Laboratory animals	All mice used were males in C57BL/6N background with normal body weight. Mice were implanted with the electroencephalogram (EEG)/electromyogram (EMG) electrodes at the age of 8-10 weeks, and EEG/EMG signals were recorded during 12-20 weeks. Age-matched control and treatment group of animals were used for each experiment.
Wild animals	The study did not involve wild animals.
Field-collected samples	The study did not involve samples collected from the field.